Influence of a PCM layer on the thermal performance of a firefighting protective clothing assembly

Integrated Masters in Chemical Engineering

by:

Jorge André Fonseca Malaquias

Institution(s) where the research was performed:

Laboratory of protection and Physiology (401)

EMPA St. Gallen – Switzerland

Centro de estudos de fenómenos de transporte (CEFT)

FEUP - Portugal

Institution granting the degree:

Department of chemical engineering

Faculty of Engineering, University of Porto

Supervisors:

Dr. Tiago Sotto Mayor, EMPA St. Gallen & FEUP

Prof. João Moreira de Campos, FEUP

Acknowledgments

The author would like to thank Dr. Tiago Sotto Mayor for his support on the build – up of this master thesis. Acknowledgments are also due to prof. João Campos for his availability to cooperate also on the build – up of this work.

The author would also like to acknowledge EMPA, for its financial support and the opportunity to elaborate a master thesis.

The author would also like to thank all the great people in EMPA and CEFT for which it was a pleasure to work with.

Abstract

PCMs (phase change materials) are recognized for their sharp melting points and high latent heats of fusion. This makes them attractive when it comes to the storage/release of heat. Firefighters usually encounter high energy heat fluxes for which the incorporation of PCMs into a firefighting protective clothing garment assembly is justified.

In this thesis, the main variables (latent heat, mass, melting temperature, PCM layer position) which influence the performance of a PCM in a latent heat thermal energy storage system (being the firefighting garment assembly in this case), were subject to an exhaustive numerical parametric study. The firefighting protective clothing assembly (FFPC) was subject to three exposure scenarios, usually encountered by firefighters. Data on thermal performance as well as design recommendations were obtained.

For all three exposure scenarios, it was found that the PCM layer should be placed as close to the exterior as possible to mitigate high temperatures in the FFPC. Melting temperature should be high enough not to melt at body temperature, but also low enough to promote the melting of the PCM. Latent heat and mass should be as high as possible as more incoming energy is absorbed as latent heat.

Keywords: PCM, variables, FFPC, flux, performance

Table of Contents

Nomenclature

λ	PCM Latent heat	[kJ/kg]
m	PCM mass	[kg]
T_m	PCM melting temperature	[ºC]
d	PCM layer position	[mm]
t_{44}	Time for skin to reach 44 ºC	[s]
t_{55}	Time for skin to reach 55 ºC	[s]
τ_{44}	Relative time for skin to reach 44 ºC	[%]
τ_{55}	Relative time for skin to reach 55 ºC	[%]
E	Total accumulated energy	[kJ]
E_λ	Latent heat accumulated energy	[kJ]
$E_{\lambda,total}$	Total latent heat available	[kJ]
T	Temperature	[ºC]
x	Spatial co-ordinate	[m]
C	Specific heat	[J/(kg·K)]
C_{app}	Apparent specific heat	[J/(kg·K)]
C_{PCM}	Specific heat of PCM	[J/(kg·K)]
ρ	Density	[kg/m^3]
k	Thermal conductivity	[W/(m·K)]
G	Blood perfusion rate	[s^{-1}]
L_{PCM}	PCM layer width	[mm]
ΔT_m	Mushy region	[K]

1. Introduction

Phase change materials (PCMs) is a term used to refer to any material in which its latent heat of fusion is of potential practical use in the storage/release of heat energy (Agyenim et al., 2010; Sharma et al., 2009; Tyagi & Buddhi, 2007; Zalba, 2003). These materials essentially fall into two major groups: inorganics and organics (Sharma et al., 2009; Zalba, 2003).

Organic PCMs mainly include paraffins composed of different carbon chains which are related with the fusion temperature of the PCM. Other organics include alcohols and acids. They tend to have a fusion enthalpy surrounding the 100-200 kJ/kg and densities in the order of 500-1000 kg/m^3. They cover a range of melting temperatures in the order of 4 – 70 ºC. A low conductivity is also associated to them typically in the range of 0.1-0.3 W/m*K (Sharma et al., 2009; Zalba, 2003) .

Inorganic PCMs on the other hand, refer mainly to hydrated salts and eutectics. They tend to have higher enthalpies of fusion (200-300 kJ/kg) and densities (1000-2000 kg/m^3) when compared to organics.They also tend to have higher thermal conductivities (0.5- 0.7 W/(m*K)) (Pielichowska & Pielichowski, 2014; Sharma et al., 2009; Zalba, 2003) .

Typically a PCM is believed to have a high potential of application if it has certain characteristics. Such characteristics include (Agyenim et al., 2010) :

- Possess a high latent heat, to be able to absorb large amounts of energy
- Have a melting temperature in the temperature operating range so that latent heat can be made use of (i.e. so that the PCM melts/freezes)
- Small volume changes with respect to the phase change, so that its encapsulation can be effectively achieved
- High conductivity to promote heat transfer towards the PCM
- Non-degradable thermal properties (i.e. latent heat) with respect to thermal cycling. Also little or no subcooling in the freezing process

- Non-poisonous to the environment

There is a tendency to have practical issues when Organic PCMs are to be implemented as they possess a lower enthalpy of fusion, tend to be highly flammable, and have a low thermal conductivity. However their thermophysical properties do not degrade considerably with thermal cycling and they present little subcooling. On the other hand, Inorganic PCMs possess high conductivities and latent heats, however subcooling issues arise when exposed to thermal cycling. Several solutions have been proposed to diminish the disadvantages related to organic and inorganic PCMs, such as adding thickening and nucleating agents to prevent hydrated salts from precipitating and diminish sub-cooling respectively, or adding flame retardants and carbon fibers to paraffins to increase thermal conductivity. However their success has been rather limited since any of these solutions implies sacrificing a part of their beneficial properties or even introducing other problems such as the precipitation of certain nucleating agents.(Farid et al., 2004; Pielichowska & Pielichowski, 2014; Zalba, 2003).

1.1 PCM Applications

The dimensioning of a Latent Heat Thermal Energy Storage (LHTES) usually involves knowledge of two major areas, namely its heat transfer characteristics, and the materials from which it is made of (Zalba, 2003). These two areas are inter-related as, on one hand it has to be determined if the LHTES provides the necessary means to effectively manage heat transfer in the area of application, and at the same time if the materials to be employed are able to achieve such performance without any practical problems. It has been shown that the four major variables which influence the performance of a LHTES with respect to its PCM are: latent heat, melting temperature, position, and mass (Bühler et al., 2013; Gao et al., 2010).

The development of LHTES using PCMs has been essentially motivated by the merge of energy crises (Agyenim et al., 2010). PCMs have thus been subject to a substantial number of studies both numerically and experimentally, and have been applied in vast areas such as in solar panels and construction (Zalba, 2003). However over time, in the context of LHTES, PCMs found themselves in applications which were not directly related to the mitigation of energy consumption but yet were seen as a

potential suitable solution to manage heat accumulation (Zalba, 2003). Applications such as in electronics, textiles, space hardware and others emphasize this aspect.

The incorporation of PCMs into textiles justifies itself with the promissing ability to positively influence the microclimate of the human body in thermal stressfull situations (Pause, 2010).

1.2 Modelling phase change

The first model to be formulated that described the melting and freezing of a given material, was the stefan model (H. Hu & Argyropoulos, 1999). The one–phase stefan model consists of assuming the fourier equation along the liquid phase and that at the phase change boundary, all the heat that reaches it through conduction, is used to melt the solid, if the imposed temperature on the PCM is higher than its melting temperature. The solid phase by its turn is always assumed to be at the melting temperature. The two-phase stefan problem adds the solving of the fourier equation to the solid phase, being the later assumption not needed. The condition assumed at the phase change boundary is that, part of the heat that reaches the phase change boundary, is transmitted towards the solid –phase.

A fact that limits the widespread use of the stefan model is its moving boundary conditions (moving phase change boundary). This implies that, the fourier equations with respect to the liquid and solid phase, have varying domain solving regions with time which are not readily known. This makes it hard to numerically solve the model. Also discontinuities in physical properties in the phase change boundary create added numerical problems (Dutil et al., 2011).

These difficulties, led to alternative formulations of the phase change problem, essentially weak formulations were employed to avoid the difficulties associated with obeying physiscal conditions near the interface. One of such is the enthalpy formulation of the phase change problem, which provides an alternative means by taking the interface position implicitly (Voller et al., 1990). Two common forms of the enthalpy formulation are the so called apparent heat capacity method where the latent and sensible specific heats are lumped to an apparent specific heat capacity and the source term method, where the latent heat is accounted for in a separate source term (Voller et al., 1990). In this thesis the apparent heat capacity form was utilized.

1.3 Apparent heat capacity model

The generic heat transfer equation assumed for a given fluid is expressed as (Comsol, 2011, p. 31).

$$\rho C_P\left(\frac{\partial T}{\partial t}+(\mathbf{u}\cdot\nabla)T\right)=-(\nabla\cdot\mathbf{q})+\tau:\mathbf{s}-\frac{T}{\rho}\frac{\partial\rho}{\partial T}\Big|_P\left(\frac{\partial p}{\partial t}+(\mathbf{u}\cdot\nabla)p\right)+Q \qquad \text{(eq.1)}$$

On the left hand side of the equation, the local acceleration and advection terms with respect to temperature change are present as the first and second terms respectively (Tu et al., p. 93). On the right side of the equation, the first term represents the diffusive term (Tu et al., 2008, p. 239). The second term accounts for viscous heating (Comsol, 2011, p. 32). The third term represents the effect of pressure work on heating of the fluid. This term tends to be small for low Mach numbers (Comsol, 2011, p. 33). The fourth term accounts for any other heat sources present in the system.

Assuming Fourier's law of heat conduction, the heat flux is directly proportional to the temperature gradient (Comsol, 2011, p. 32);

$$q_i=-k\frac{\partial T}{\partial x_i} \qquad \text{(eq.2)}$$

ignoring heating due to viscous effects and assuming negligible pressure work (Comsol, 2011, p. 33) eq. 1 becomes;

$$\rho C_P\frac{\partial T}{\partial t}+\rho C_P\mathbf{u}\cdot\nabla T=\nabla\cdot(k\nabla T)+Q \qquad \text{(eq.3)}$$

furthermore if only one dimensional conductive heat transfer is considered, the expression simplifies further to (Comsol, 2011, p. 33):

$$\rho C_P\frac{\partial T}{\partial t}=\frac{\partial}{\partial x}\left(k\frac{\partial T}{\partial x}\right)+Q \qquad \text{(eq.4)}$$

This is known as the Fourier equation. The apparent heat capacity method is obtained by imposing a specific heat which depends on temperature and includes the latent heat effect during the phase change:

$$\rho C_{app} \frac{\partial T}{\partial t} = \frac{\partial}{\partial x}\left(k \frac{\partial T}{\partial x}\right) + Q \qquad \text{(eq.5)}$$

where

$$C_{app} = \frac{exp\left(-\frac{T - T_m}{T_0}\right)^2}{T_0\sqrt{\pi}} + C_{PCM} \qquad \text{(eq.6)}$$

To see the derivation of the C_{app} expression (equation 6) please refer to annex D.

1.4 PCM application to FFPCs assemblies

Firefighters are usually exposed to high levels of thermal stress which negatively affect their microclimate (Barr et al., 2010).It is therefore of practical interest to see if the inclusion of a PCM in a Firefighting protective clothing (FFPC) assembly, augments its thermal performance. The idea of incorporating PCMs into Firefighting protective clothing is not new. Rossi & Bolli (2005) incorporated a PCM coated layer FFPC assembly and tested it for various exposure scenarios and PCM layer configuations. They found that the inclusion of a PCM layer in an FFPC has great potential in increasing the pain alarm time and that a configuration closer to the skin is more beneficial to thermal performance. Zhu et al. (2015) also studied the incorporation of a PCM coated layer into a FFPC assembly and tested it also for various exposures. They used PCMs with different melting temperatures and almost equal remaining thermophysical properties, and also varied the configuration. They concluded that a melting temperature surrounding 52 ºC and a configuration closer to the skin is beneficial to thermal performance. Y. Hu et al. (2012) numerically studied the inclusion of a PCM layer in an FFPC assembly including the various skin layers, assuming one-dimensional heat transfer behaviour. The authors varied the mass of the PCM layer and its position and submitted the FFPC-skin assembly to a temperature function with time. They concluded that a higher mass and position towards the skin decrease the temperatures developed along the FFPC through time. Hunag et al. (2010) numerically studied the influence of melting temperature on the thermal performance of a FFPC-skin system assuming the same boundary condition as the former reference. The authors, unlike the ones

mentioned above, considered the effect of sweat on thermal performance. They concluded that PCM melting temperature had an effect on the thermal performance and that there is an optimum. Phelps & Sidhu (2015) numerically studied the effect of adding an extra air layer to the FFPC-skin system incorporating a PCM.

Eventhough substantial research has been done on the incorporation of PCMs to a FFPC assembly, the justifications behind the results obtained are questionable. The mentioned studies above consider a limited number of configurations of the variables at stake (latent heat, PCM position, melting temperature, mass of PCM). Also, limited data is shown to draw definite conclusions on the thermal performance of the FFPC assembly.

1.5 Outline and scope of thesis

This thesis builds-up on the works mentioned above so as to draw guidelines when it comes to the incorporation of PCMs into a FFPC assembly. No air gaps are considered and radiant exchange between layers is neglected, being conduction the main heat transfer mechanism. Thesis is essentially divided in 3 parts: first the materials and methods used to obtain the results are discussed, followed up by the exposure of the results and their critical analysis. A conclusion is presented at the end highlighting the important finding of the work.

2. Materials and Methods:

Simulations were performed in COMSOL Multiphysics 5.1 in a computer with 2 processors Intel® Xeon® CPU E5-2620 v2 @ 2.10 GHz . The computer has a total installed memory (RAM) of 42 GB. The *heat transfer in fluids* physics *was* used to perform the required simulations.

2.1 Case study

A typical garment-skin system of a firefighter was assumed, to analyse the effect of PCMs in enhancing thermal protection (G N Mercer & Sidhu, 2008; Phelps & Sidhu, 2015). Boundary 1 (Figure 1) was subject to a sudden heat flux for a certain amount of time. Three fluxes were chosen to reflect the different scenarios that firefighters can encounter: 84 kW/m^2 for 8 s, 12 and 5 kW/m^2 for 5 min (Phelps & Sidhu, 2015). After the exposure the boundary was isolated. For the different fluxes, variables associated with the PCM layer were varied independently. Position of PCM layer, melting temperature, latent heat, and mass of PCM were varied and analysed to study their effects on the temperature profiles obtained. These variables are reported to have an influence in the thermal performance of the PCM. Parameter values that were simulated can be found in table 5.

2.2 General Assumptions

All simulations were run using the apparent heat capacity method. The *heat transfer in fluids* module was activated to implement the method. One-dimensional heat conduction was assumed to be the major heat transfer mechanism, neglecting radiation between the garment layers and convection. Heat removal through blood circulation was assumed in the dermis and subcutaneous layers (Y. Hu, Huang, et al., 2012; G N Mercer & Sidhu, 2008; Phelps & Sidhu, 2015). Air gaps between the garment layers and the skin were neglected to simulate the worst possible case in terms of thermal performance (Geoffry N. Mercer & Sidhu, 2009).

Regarding the garment assembly materials, the following assumptions were made:

- Constant thermophysical properties throughout the process of the various layers as the temperature ranges involved are not very wide. Regarding the PCM, the

thermophysical properties were assumed to be the same and constant for both phases (McCarthy & Marzo, 2012; G N Mercer & Sidhu, 2008; Geoffry N. Mercer & Sidhu, 2009);

- The latent heat associated with the PCM was obtained by DSC (Differential scanning calorimetry). The resulting thermogram in turn was approximated by a function by a minimizing square technique where the size of the mushy region (i.e. temperature interval where the phase change is assumed to happen) was considered the floating variable. This function was then used and adapted for all simulation cases (Y. Hu, Huang, et al., 2012; Hunag, Li, Tong, Yang, & Zhang, 2010; Phelps & Sidhu, 2015). The other variables were set by the data provided in the paper that reported the DSC curve (A. A. F. Al-Hamadani & Shukla, 2012). Only the charge DSC curve was assumed for the whole process (please see annex C for more information on this assumption);

- Blood perfusion rates were assumed constant in the dermis and subcutaneous layers (Y. Hu, Huang, et al., 2012; Hunag, Li, Tong, Yang, & Zhang, 2010; Phelps & Sidhu, 2015);

- Core body temperature is assumed constant at 37 ^{o}C (Y. Hu, Huang, et al., 2012; Hunag et al., 2010; G N Mercer & Sidhu, 2008; Phelps & Sidhu, 2015).

2.3 Parameters

Several quantities were introduced in the FEM platform as parameters to give them a physical identification and also allow them to be used in parametric sweeps if needed.

2.4 Materials

Properties of the different garment layer materials are shown in Table 3 (Annex A). The firefighting garment assembly may also contain a moisture barrier (Y. Hu, Huang, et al., 2012), which is not accounted for in this work. Such might be done at a later stage as in principle, the addition of an extra thermal resistance does not affect

the qualitative and quantitative conclusions on the variables which influence the thermal performance. This assumption was also considered by various other authors (Y. Hu, Huang, et al., 2012; G N Mercer & Sidhu, 2008; Phelps & Sidhu, 2015).

2.5 Geometries and boundary conditions

Geometries were built using the geometry node in the FEM platform. Simple primitive elements were used to build the final case geometries. Dimensions of the different primitives were defined in the geometry settings window, and also their position relative to the origin. The dimensions for each case are shown in Table 1.

Table 1: Geometry dimensions

Domain dimensions [mm]
L_{Outer} = 0.7 L_{PCM} = 1.0 L_{Inner} = 0.95 $L_{Epidermis}$ = 0.08 L_{Dermis} = 2 L_{Subcut} = 10

Table 2: Boundary conditions (named according to Figure 1: Geometry with boundaries 1 and 2 with domain sets α and β representing the garment and skin layers respectively)

Boundary	1	2
Case A1	Heat flux 84 kW/m^2 for 8 s	Constant temperature 37 ºC
Case A2	Heat flux 12 kW/m^2 for 5 min	Constant temperature 37 ºC
Case A3	Heat flux 5 kW/m^2 for 5 min	Constant temperature 37 ºC

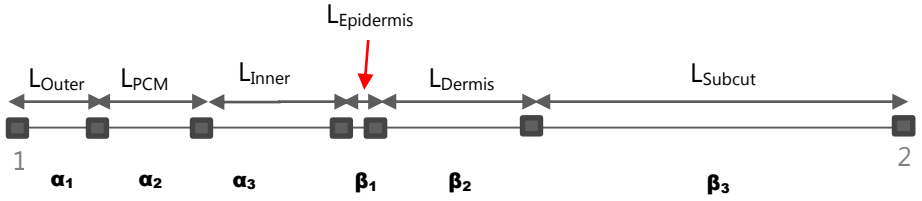

Figure 1: Geometry with boundaries 1 and 2 with domain sets α and β representing the garment and skin layers respectively

2.6 Domain conditions

Domain set α (clothing layers) was considered to be at an initial temperature of 34 ºC. Domain set *B* (skin layers) was considered to be at a temperature gradient between 34 and 37 ºC, where boundary 2 (core) was at 37 ºC.

2.7 Meshing

Meshing was done in the FEM platform under the Mesh node. Mesh parametrization was performed whenever possible to find grid independent solutions (Wilkes, 2009, pp. 107–111). In cases where such was not possible or inconvenient, studies with different meshes were added (see annex B for more information on meshes used).

2.8 Solver configuration

Solvers and settings were kept as default for the different cases. In cases A1 through A3, the Backward differentiation formula (BDF) solver was utilized due to the stiff nature of the differential equations which describe the PCM thermal behavior (Solomon & Alexiades, 1993). A minimum and maximum time step order was chosen as 1 and 2 respectively to delay dissipatedness and promote stability. A *strict* criterion for the time steps taken by the solver was also imposed with a maximum time step limit. In this way, one can be sure that the phase change phenomena are correctly accounted for and control of the time step is ensured. Absolute and relative tolerances were used to control the initial time steps as these tend to be smaller due to the varying boundary conditions at the beginning of the process.

2.9 Convergence criteria

For this type of application, energy balance convergence criteria can be harder to define. Gao et al. (2010) reported that a 6 W/m^2 flux developed between the body and the PCM in its change of phase in a given garment assembly, did not influence body

surface temperature. Other authors (Shim et al., 2001) reported sinusoidal variation of the heat flow from the body with an amplitude of 30 W for periods close to 15 min, and reported that this had negligible effect on the body temperature. As will be seen in the results, the major imbalances happen in the beginning of the process where the boundary conditions contain steep gradients which have to be detected by the solver in order to obtain accurate results. It is mainly in these moments that the imbalances happen but their influence on the process is negligible due to their short duration. Hence, energy balance convergence was declared whenever the absolute difference between the accumulated heat in the whole domain and heat flow that goes through boundary 1 (see Figure 1) was less than 50 W/m^2 for a period of time of no more than 3 s. But then again, the criteria could be less strict due to the reasons mentioned above.

3. Results and Discussion:

As it is known, a PCM has the capability of storing energy in the form of latent heat (and release it) at an almost if not constant temperature (Sharma et al., 2009). When the firefighting assembly is exposed to a heat flux, the PCM melts absorbing part of the energy as latent heat. After the exposure, the temperature of the PCM drops, making it resolidify and hence release latent heat energy into the garment-skin system.

A PCM changes phase in its melting temperature T_m if it is pure or if no subcooling is present. If it is not pure, or subcooling phenomena are present, it will change phase in a small temperature range called the mushy region which is limited by the solidifying temperature (T_s) which is the temperature in which it starts changing to liquid and the liquifying temperature (T_l) which is the temperature when it ends changing to liquid, when charged (Zalba, 2003).

So the presence of a PCM in the firefighting garment assembly allows for heat absorption in the form of latent heat in, or in the vicinity of the melting temperature (T_m). Hence, during exposure, an enhanced portion of the energy that comes into the firefighting garment assembly is expected to be stored at a temperature close to T_m in the PCM layer. This happens only if the PCM reaches at least T_l, during the exposure.

To see how this affects the temperature profiles in the garment-skin system, a simulation was initially carried out assuming that the PCM layer did not have any latent heat (λ = 0 kJ/kg) so it would act purely as a thermal resistance. Latent heat was then included to see its effect on the temperature profiles obtained. An interesting thing to analyse would be to see if the thermal resistance associated with the PCM has any meaningful effect on the temperature profiles obtained. Hence a third simulation was performed where the conductivity of the PCM was assumed to be very high (k_{PCM} = 1000 W/(m·K)). More details on the parameters used to perform these simulations can be found in Annex C.

The exposure of Case A1 (84 kW/m^2 for 8 s) was used as the boundary condition for the simulations that follow. Figure 2 shows the temperature histories obtained at the indicated boundaries for the various latent heat and PCM thermal conductivity configurations indicated. Figure 3 shows the temperature histories at the Epidermis/Dermis layer in more detail. As can be seen, an increase in latent heat (λ)

originates a decrease in the temperatures obtained (Figure 2a and b, Figure 3). As expected, when latent heat is involved, more energy is absorbed at a lower temperature ($T_s < T < T_l$) which in turn originates a decrease in the temperatures obtained throughout the garment-skin system (Figure 2a and b, Figure 3).

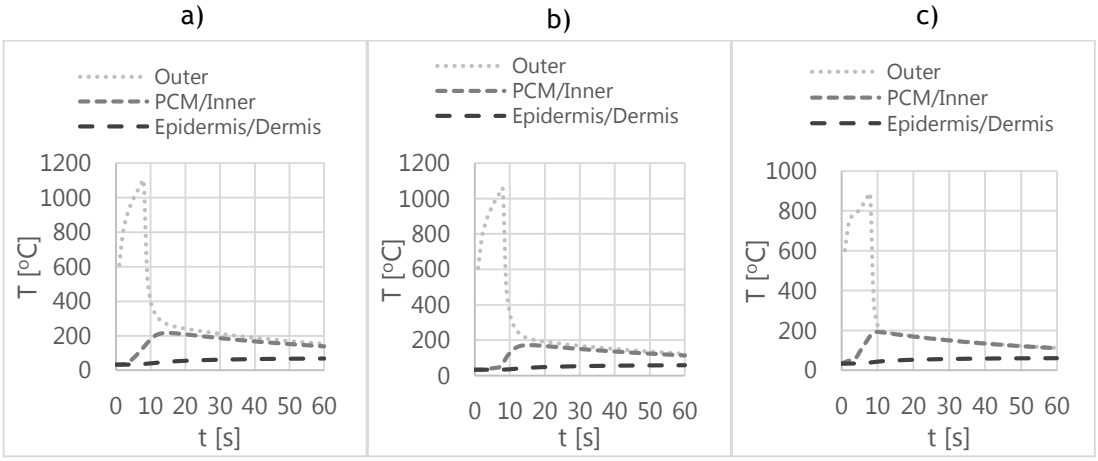

Figure 2: Temperature profiles obtained in different positions across the garment-skin system, for an exposure of 84 kW/m² for 8 s (Case A1) a) λ = 0 kJ/kg, k_{PCM} = 0.16 w/(m·K) b) λ = 199.8 kJ/kg, k_{PCM}= 0.16 w/(m·K) c) λ = 199.8 kJ/kg, k_{PCM} = 1000 w/(m·K)

When the thermal conductivity of the PCM (k_{PCM}) is increased to a very high value, its thermal resistance can be considered negigible. This was done to compare the effect of the thermal resistance relative to that of the phase change, on the temperature histories obtained for the various positions. Figure 2b and Figure 2c show the temperature profiles obtained when k_{PCM} = 0.16 W/(m·K) and k_{PCM} = 1000 W/(m·K) respectively, maintaining everything else constant. As shown, an increase in $k_{PCM,}$ causes a decrease in temperature in the outer layer, and an increase in the PCM/Inner and Epidermis/Dermis layers (Figure 2c, and Figure 3). This is reasonable as a decrease in thermal resistance originates less steep thermal gradients in the garment-skin system, making the outer positions, facing the flux, to decrease in temperature, and the ones in the inner positions to increase in temperature.

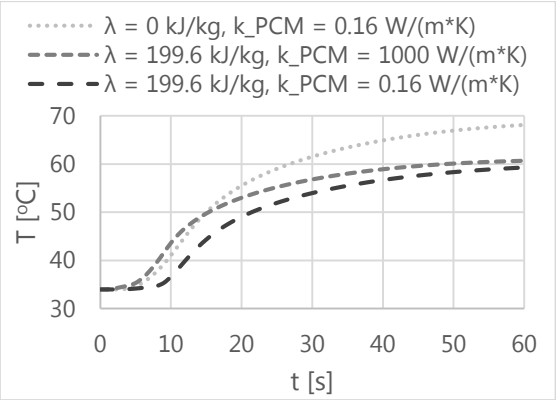

Figure 3: Temperature histories at the Epidermis/Dermis boundary.

From Figure 2b and c and Figure 3, it is evident that the thermal resistance associated with the PCM plays a considerable role in the temperature profiles obtained. This has to be accounted for if the width of the PCM layer is to be varied.

The rest of the results is divided into four sections. Each section contains the results and discussion of each of the four major variables that influence the PCM thermal performance (PCM latent heat, mass , melting temperature and position). In section 3.1, the influence of the PCM latent heat is studied. Section 3.2 deals with the influence of PCM mass. Section 3.3 describes how the PCM melting temperature influences the thermal performance of the firefighting garment assembly. Lastly section 3.4 describes how a difference in position of the PCM layer influences the thermal performance.

3.1 PCM Latent heat influence

Latent heat is the energy associated with a phase change. The big advantage of using this form of heat to store and release energy, is the fact that it is done at an almost, if not constant temperature. That is a typical characteristic of a phase change. For the firefighting garment assembly,when the external heat source is high enough to make the PCM melt, this means that part of the heat flux that enters the garment-skin system is stored as latent heat at an almost constant temperature. This means that less heat from the external source is stored as sensible heat in the garment-skin system. Therefore, lower temperatures are obtained in the garment-skin system (Figure 2a and

b, and Figure 3). So, naturally, a high latent heat is usually recommended to store large amounts of energy in the PCM (Sharma et al. 2009; Zalba, 2003).

Physically it is easy to understand the influence of increasing the latent heat in a PCM. As long as the heat flux imposed is big enough to melt the PCM, a higher latent heat implies that higher amounts of energy are stored as latent energy as opposed to being stored in the form of sensible heat (higher temperatures). However when a PCM layer is incorporated into a firefighting garment assembly, and subjected to an external heat source variable with time, the effect of the PCM in the temperature profiles obtained is rather complex due to thermal inertia effects. To the knowledge of the author, the influence of latent heat has not been directly studied yet under such a scenario. Hence, it will be studied in this section.

Simulations were carried out using the garment-skin system as outlined in Figure 1. For each of the simulations, a different value of latent heat associated to the PCM (λ) was considered (for the specific values of λ considered in the simulations please refer to annex C). Temperature histories at the epidermis/dermis layer were then obtained. Of particular interest, is the time that it took for the epidermis/dermis layer to reach 44 ºC and 55ºC, as these are the temperatures at which a first and second degree burns usually occur, respectively (McCarthy & Marzo, 2012). For the time it takes for the epidermis/dermis layer to reach 44 ºC, a variable is defined (i.e. t_{44}). The same is done for the time it takes to reach 55 ºC (i.e. t_{55}). These two parameters are of particular importance since they reflect the thermal performance achieved with a given configuration, that is, a given latent heat and exposure type, with respect to the current analyses.

Figure 4a, b, and c show the temperature histories obtained at the epidermis/dermis layer for the indicated latent heats for cases A1, A2, and A3. For all cases throughout time, the temperature at the epidermis/dermis boundary first increases because of the exposure, as expected. For cases A2 and A3 the simulations were prolonged for enough time to see the temperature decrease, as the heat flows into the body which is at a lower temperature (t > 300 s in Figure 4b and c, and Figure 7b). For case A1, this is not visible in the simulated time (Figure 4a). As can also be seen, the exposure of Case A2 results in higher temperatures than those of Cases A1 and A3 (Figure 4). This is because

Case A2 implies exposure of the garment-skin system to a higher amount of energy from the external heat source than in the other two cases (see Table 2).

For all cases, it is verified that an increase in latent heat originates a decrease in the temperatures obtained at the epidermis/dermis boundary (Figure 4). As expected, a higher latent heat implies that more heat is stored in the form of latent rather than sensible energy in the garment–skin system. Figure 5 shows the latent heat accumulated in the PCM domain for the various cases and PCM latent heats considered (to see how latent heat is computed please refer to annnex D). As shown, for all cases, an increase in the PCM latent heat implies that a greater portion of the incoming heat flux is stored as latent heat (Figure 5). Figure 6 shows the used percentage of total available latent heat that is offered by the PCM, for the various latent heats considered (to see how it's computed please refer to annex D). As can be seen, in all cases, all of the PCM latent heat is used to absorb energy. Hence, the PCM fully melts for all cases and latent heats considered. Figure 7b shows the temperature profiles obtained along the garment–skin system for t = 8 s for case A1 and t = 300 s for cases A2 and A3, for the indicated latent heats. As shown, throughout the whole domain, a lower temperature is registered, when the latent heat of the PCM increases.

So, as an increase in latent heat originates lower temperatures in the garment-skin system throughout time (Figure 4 and Figure 7b), this will have an impact on the time it takes for the epidermis/dermis boundary to reach 44 ºC and 55 ºC. Figure 8a shows the time it takes for the epidermis/dermis boundary layer to reach 44 ºC (t_{44}) and 55 ºC (t_{55}). As shown, Case A1 always origins the shortest t_{44} and t_{55} regardless of the latent heat considered, followed by cases A2 and A3, respectively. Also, for all cases, there is, as expected, a tendency for t_{44} and t_{55} to rise with increasing latent heat. From this graph it is very hard to visualize any other phenomena, such as change in gradients of the curves. So, relative times (τ_{44} and τ_{55}), are defined relative to the shortest t_{44} and t_{55} obtained, respectively (see Annex D for details). Figure 8b shows the relative times that it takes for the epidermis/dermis layer to reach 44 ºC (τ_{44}) and 55 ºC (τ_{55}). As can be seen, for *Case A1_τ55* (that is, τ_{55} for case A1), when the latent heat associated with the PCM increases beyond 150 kJ/kg (λ > 150 kJ/kg), τ_{55} (that is, the relative time it takes for the epidermis/dermis layer to reach 55 ºC) increases in a more than proportionate way. This is because not all of the PCM melts during the exposure time (0 s < t < 8 s; λ = 300 kJ/kg and t > 8 s in Figure 5a). This is also evidenced

in Figure 7b if the two lines that representing the temperature profiles at t = 8 s for λ = 100 kJ/kg and λ = 300 kJ/kg are considered. As shown, for the case where λ = 300 kJ/kg, the PCM (which is in the range 0.0007 m < x < 0.0017 m), has not completely melted since in its domain there are positions which still have a temperature between T_s and T_l (being 40.9 ºC and 50.9 ºC in this case, respectively). This means that the rest of the PCM will be used to absorb the heat that is accumulated in the garments after the end of the exposure, thus delaying the burns, i.e increasing τ_{55}. The outer shell is the garment layer with the highest temperatures (Figure 7b, 0 m < x < 0.0007 m). So the fact that the PCM does not melt completely, means that it still has a very high potential inertia (Annex figure 1). Therefore, the energy associated with the high temperatures that are present after the exposure will be absorbed as latent heat (rather than being transferred to the skin). Hence, the increase in the relating time to second degree burn (t_{55} or τ_{55}) obtained in Figure 8 for latent heats above 150 kJ/kg. It can be conluded that, from such latent heat upwards, the PCM does not completely melt during the exposure, and that part of it is used to absorb the energy present after the end of the exposure. This phenomena will be more apparent when the PCM mass is varied as discussed next.

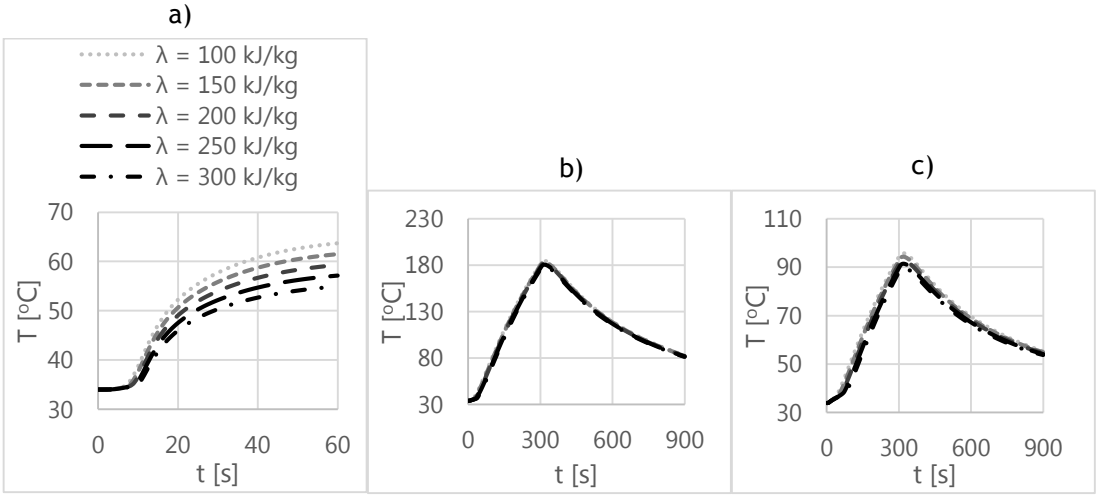

Figure 4: Temperature histories at the Epidermis/Dermis boundary for cases a) A1 (84 kW/m² for 8 s) b) A2 (12 kW/m² for 5 min) and c) A3 (5 kW/m² for 5 min)

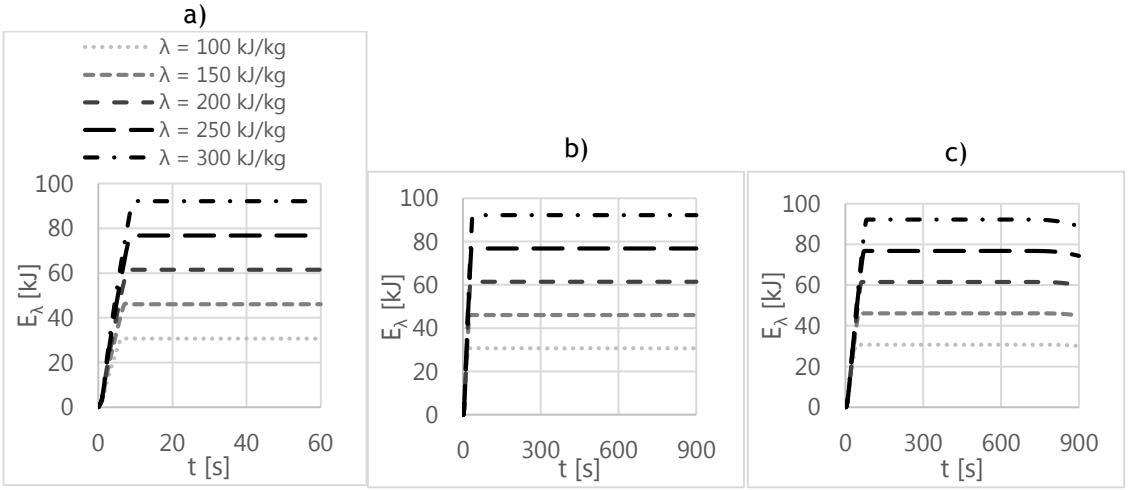

Figure 5: Latent energy accumulated in PCM domain for cases a) A1 (84 kW/m² for 8 s) b) Case A2 (12 kW/m² for 5 min) c) Case A3 (5 kW/m² for 5 min)

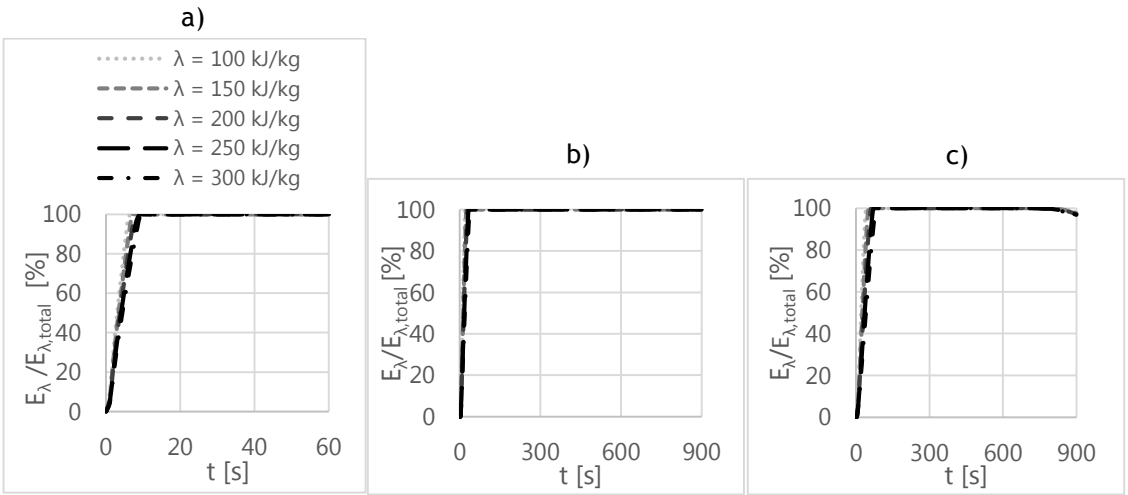

Figure 6: Total latent energy accumulated in PCM domain in terms of percentage relative to total latent heat available ($E_{\lambda,total}$ = mλ) for cases a) A1 (84 kW/m² for 8 s) b) A2 (12 kW/m² for 5 min) c) A3 (5 kW/m² for 5 min)

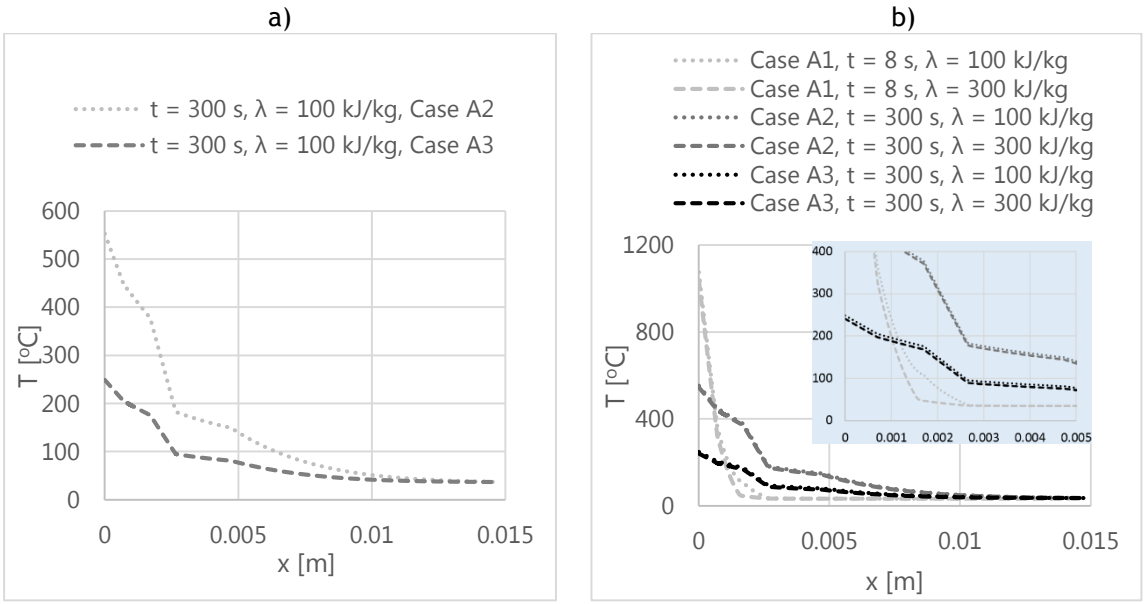

Figure 7: a) Temperature profiles in the garment-skin system for Cases A2 (12 kW/m² for 5 min) and A3 (5 kW/m² for 5 min) assuming a latent heat (λ) of 100 kJ/kg b) Temperature profiles in the garment-skin system for the various cases, times (t) and latent heats

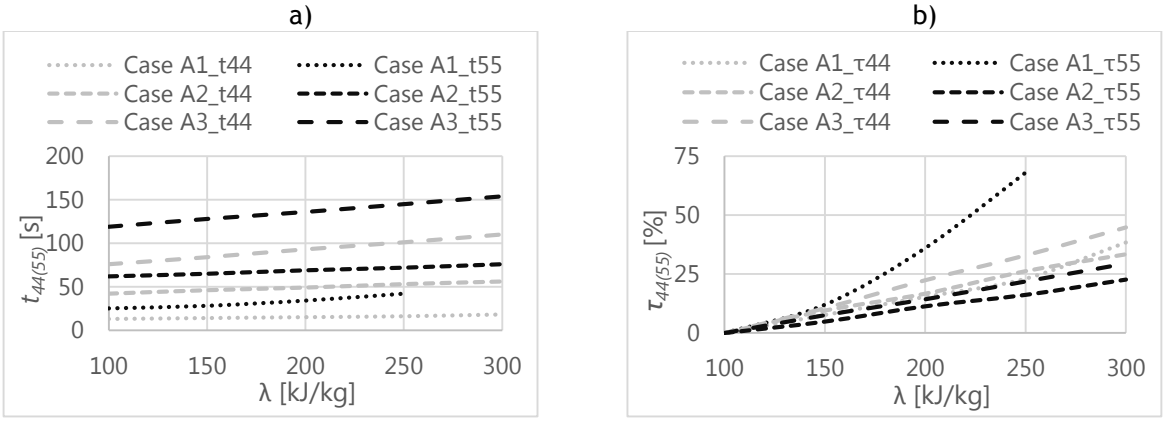

Figure 8: Absolute and relative time to first (t_{44} and τ_{44}, respectively) and second (t_{55} and τ_{55}, respectively) de-gree burns at the skin; a) Absolute time to burns b) relative time to burns

3.2 PCM mass influence

As seen in section 3.1, an increase in the PCM latent heat originates an increase in the PCM latent energy. It also originates an increase in the times to first (t_{44}) and second (t_{55}) degree burns (Figure 8). An increase in the PCM mass also originates an increase in the latent energy available (Table 5). Hence, a similar effect should be observed. An increase in PCM mass is expected to decrease the temperatures obtained throughout the garment–skin system, and hence to increase time to burns (t_{44} and t_{55}).

The influence of PCM mass on the temperature profiles obtained throughout the garment–skin system (Figure 1) has been studied to a very limited extent by (Y. Hu, Huang, et al., 2012). The author only considered a limited number of PCM mass configurations for which it was impossible to take further conclusions on how exactly the PCM mass influenced the thermal performance.

In the present study, different PCM masses were considered up to 2 kg (House, Lunt, et al., 2013). For the calculation of the width of the PCM layer representing the mass of PCM, it was assumed that only the upper body front part of the suit was covered with PCM. Cervicale and crotch mean heights were taken from a sample of fireman (151.9 cm and 78.5 cm, respectively) and then subtracted to get a height for the upper body (Hsiao et al., 2014). Waist circumference (97.1 cm) was then multiplied by the height of the upper body to get the upper body area, and then divided by two to obtain only the area of the front part of the upper body (0.36 m^2). The upper front body area together with the PCM density and mass were then used to obtain the PCM layer width. PCM layers with up to 6.5 mm of thickness (corresponding to a mass of 2 kg) were considered. Temperature profiles along the garment-skin system for various times and temperature histories at the epidermis/dermis layer were then obtained.

Figure 9 shows the temperature histories obtained at the epidermis/dermis boundary. As can be seen, a higher PCM mass results in lower temperatures obtained at the epidermis/dermis boundary over time. This was to be expected as a higher PCM mass means that a higher latent energy is available and so more of the incoming heat can be stored as latent instead of sensible heat. To emphasize this, consider Figure 10 showing the temperature profiles obtained for the indicated masses and times, for case A1 (84

kW/m^2 for 8 s). As shown, as the mass of the PCM increases, the temperatures obtained for higher times decrease throughout the garment–skin system (e.g. Figure 10, t = 19 s). The same happens for the other two cases.

As the temperature profiles obtained differ with PCM mass, so does, surely, the energy it accumulates during the process. Figure 11 shows the total energy accumulated throughout the process (see Annex D for calculation). As shown, for all cases, there is first a rise in the energy accumulated as expected because of the exposure to the external heat source. Also, for all cases, an increasing mass increases the total energy (sensible and latent) stored in the PCM, throughout time (Figure 11).

For Case A1 (84 kW/m^2 for 8 s) after the exposure (t > 8 s), when the total accumulated energy in the PCM decreases (Figure 11, 8 s < t < 60 s) the temperature at the epidermis/dermis boundary increases (Figure 9, 8 s < t < 60 s). Furthermore, the higher the PCM mass the lower the temperature at the epidermis/dermis boundary, and the higher the energy absorbed in the PCM (Figure 12, 8 s < t < 60 s). This trend is also verified for Cases A2 and A3, but the difference being that the phenomena is now visible before the exposure is over (Figure 12b-c; 0 s < t < 300 s). This difference has to do with the elevated heat that enters in a very short time, associated with case A1.

So, the PCM mass has a clear effect on the total energy absorbed by the PCM which, in turn, affects the temperature histories obtained at the epidermis/dermis boundary (Figure 12 and Figure 9, respectively). Hence, this should also influence the times to first and second degree burns (t_{44} and t_{55}), obtained for the various PCM masses considered. Figure 14a shows the t_{44} and t_{55} obtained for the given PCM masses. As shown and expected, increasing PCM mass results in an increasing t_{44} and t_{55} (Figure 14). To see the patterns more clearly, Figure 14b shows the relative times τ_{44} and τ_{55}. As can be seen, a more than proportional increase is verified for *Case A1_τ44* for m > 200 g, and it is also verified for *Case A3_τ44* for m > 1600 g. This increase is solely due to the increase in PCM mass. To note also that when m > 200 g, for case A1, not all of the PCM melts during the exposure (t > 8 s in Figure 13a) The observed exponential increase happens because, above a certain PCM mass, not all of it melts during the exposure. This in turn implies that the heat associated with the high temperature gradients present after the exposure (x < 0.0007 m in Figure 10), is stored in the PCM as latent heat. This happens for all cases in the range of PCM masses considered except

in Case A2 since all of the PCM melts before the exposure is over (0 s < *t* < 300 s in Figure 13b) . This is similar to what happened when the latent heat was varied (Section 3.1). To note also that there are cases where the PCM does not all melt during the simulation time (e.g. *m* = 1000 g in Figure 13a, the latent heat usage does not reach 100 % in the simulation time considered, and it also wouldn't for higher times since, in this particular case for *t* > 120 s, the PCM starts solidifying, visible by a decrease in the % of heat accumulated in the PCM layer). When not all of the PCM melts and there is no more heat available to be stored into it, the PCM starts solidifying. This means that, from this point on, adding more PCM won't change the amount of latent heat stored (e.g. *m* > 800 g in Figure 12a). So the increase in τ_{44} and τ_{55} from this point on, is solely due to the enhanced thermal resistance offered by the extra PCM mass added, justifying the linear tendency then observed (e.g. *m* > 800 g in Figure 14b).

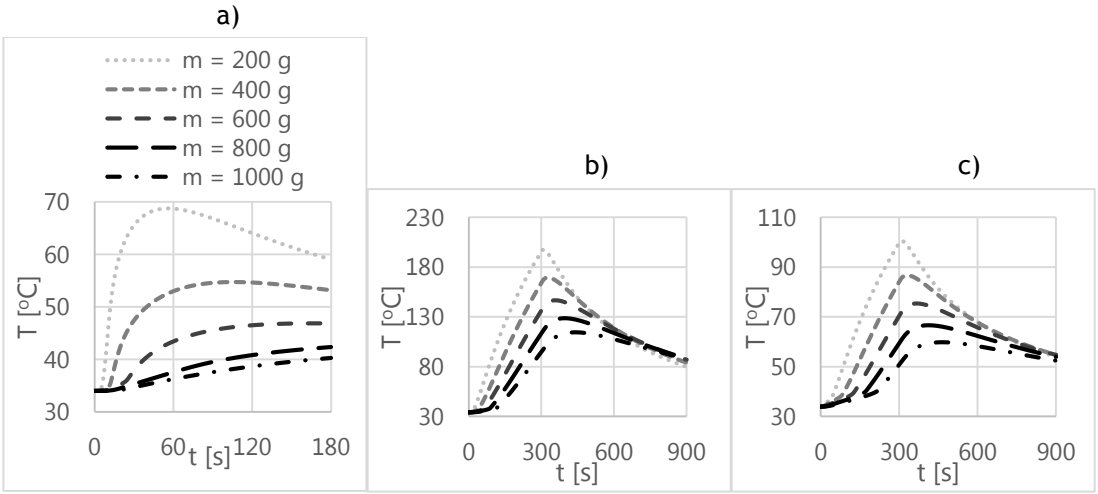

Figure 9: Temperature histories obtained at Epidermis/Dermis boundary for cases a) A1 (84 kW/m² for 8 s); b) Case A2 (12 kW/m² for 5 min); c) Case A3 (5 kW/m² for 5 min)

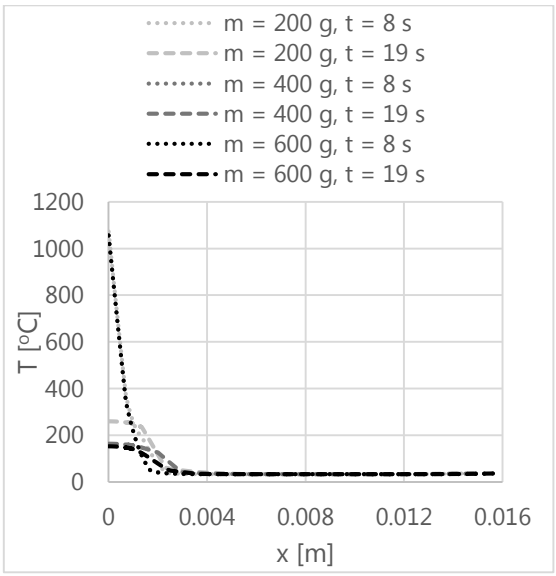

Figure 10: Temperature profiles obtained for Case A1.

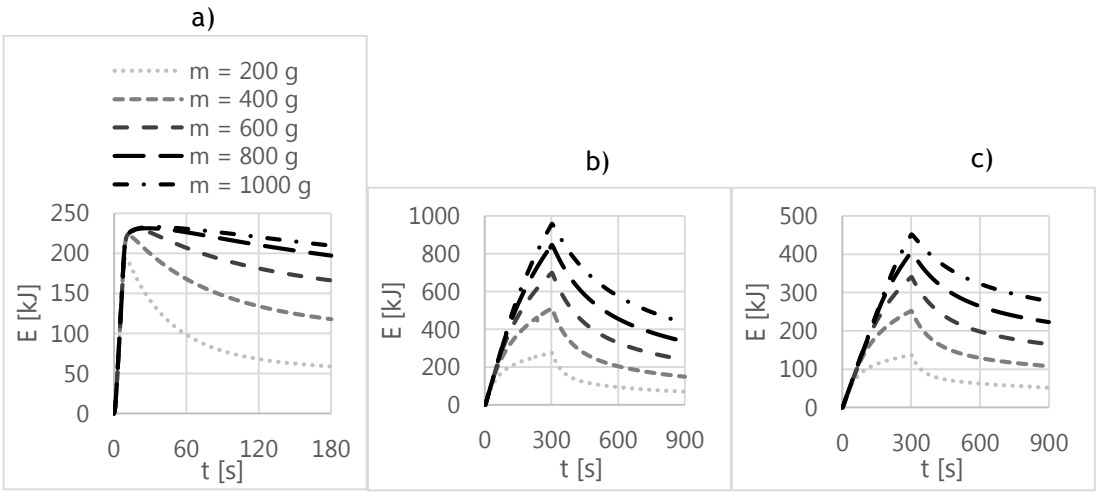

Figure 11: Total energy accumulated in PCM domain for cases: a) A1 (84 kW/m^2 for 8 s); b) Case A2 (12 kW/m^2 for 5 min); c) Case A3 (5 kW/m^2 for 5 min)

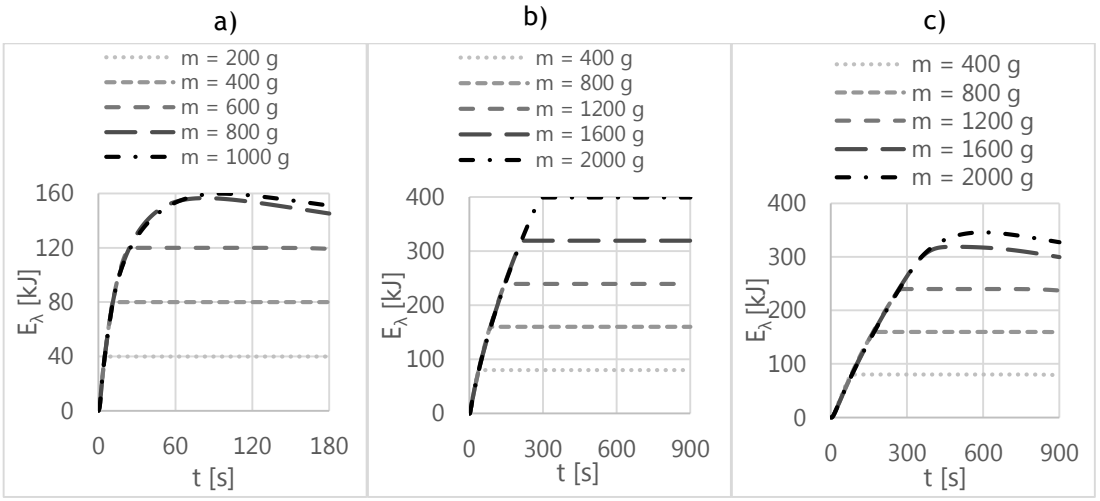

Figure 12: Latent energy accumulated in PCM domain for cases: a) A1 (84 kW/m² for 8 s); b) Case A2 (12 kW/m² for 5 min); c) Case A3 (5 kW/m² for 5 min)

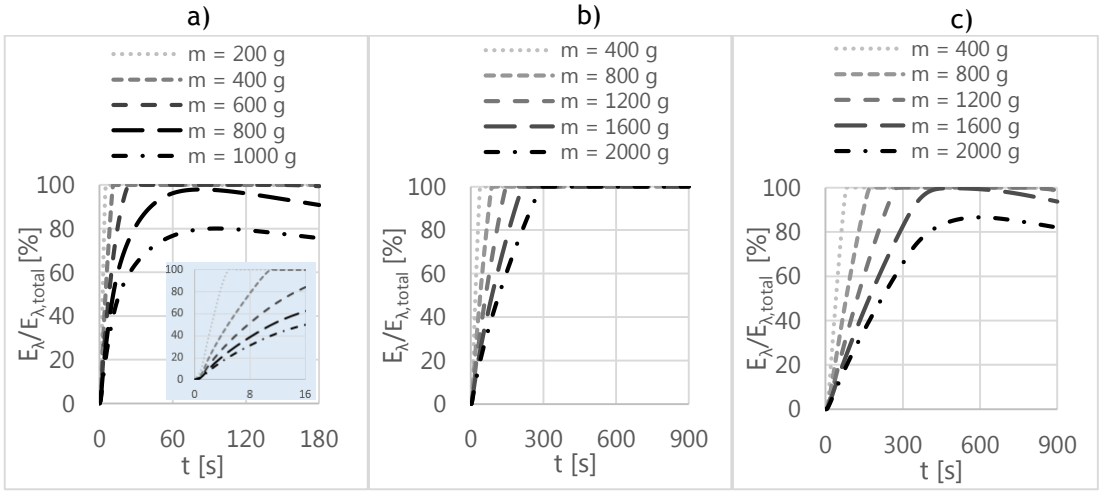

Figure 13: Latent energy accumulated in PCM domain in terms of percentage relative to total latent heat available ($E_{\lambda,total}$ = mλ) for cases: a) A1 (84 kW/m² for 8 s); b) A2 (12 kW/m² for 5 min); c) A3 (5 kW/m² for 5 min)

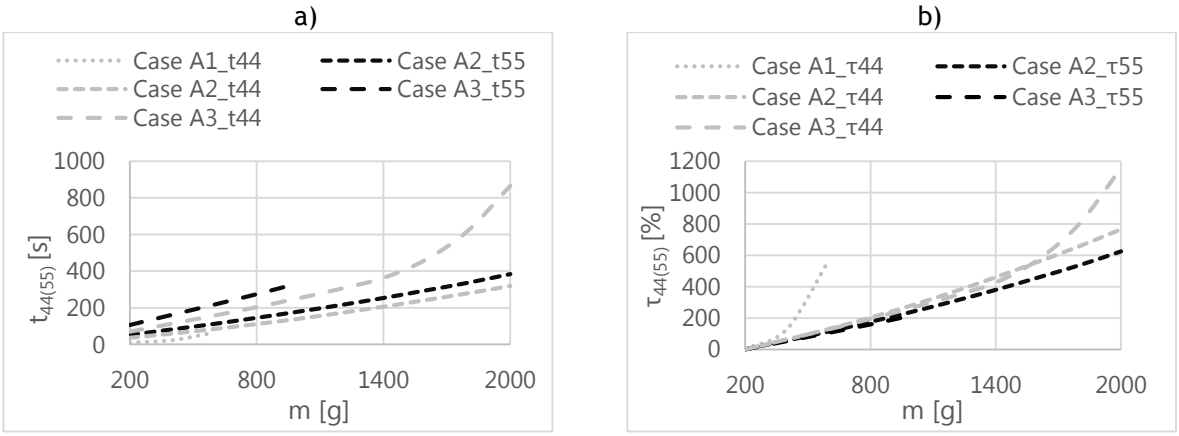

Figure 14: Absolute and relative time to first (t_{44} and τ_{44}, respectively) and second (t_{55} and τ_{55}, respectively) degree burns at the skin: a) Absolute time to burns; b) relative time to burns

3.3 Influence of PCM melting temperature

The melting temperature of a PCM is the temperature at which it changes phase, if pure. A higher melting temperature of a PCM in a given position, and for a given mass and thermophyical properties, implies that, during an exposure, it will only change phase at a higher temperature. The melting temperature of the PCM has been reported to have an influence on clothing applications involving PCMs (Gao, Kuklane, & Holmér, 2010; Hunag, Li, Tong, Yang, & Zhang, 2010). However, conclusions differ as to what the best choice of the melting temperature is. One has to keep in mind that raising the melting temperature of the PCM will make it change phase at a later time during a charge process (exposure to heat), or make it not change phase at all if, during the exposure, T_m is not reached at the PCM layer due to the low intensity of heat reaching the PCM. In the latter scenario more heat is allowed to go through towards the skin. This also implies that certain values of T_m might allow for only a partial melting of the PCM during a heat exposure. So, with very high PCM melting temperatures, less PCM melts and therefore less latent heat is used to absorb the energy from the incoming flux.

In this section, simulations were run where the melting temperature of the PCM was varied between 50 and 200 ºC (to see specific values of the parameters considered in the simulations refer to annex D). For each melting temperature, the temperature history at the epidermis/dermis layer was obtained as well as temperature profiles across the garment-skin system. This was done for the three exposure cases (Table 2). The total energy accumulated in the PCM layer during the process was also obtained.

Figure 15 shows the temperature histories obtained at the epidermis/dermis boundary. As can be seen for all cases, during the exposure, an increase in the melting temperature (T_m) originates an increase in the temperatures obtained (Figure 15a-c). But for case A1, when T_m is higher than 100 ºC, the temperature history obtained becomes significantly different. Temperatures rise dramatically at the epidermis/dermis boundary with increasing T_m. This could indicate that not all of the PCM melts during the exposure when T_m is increased. This could also mean that not all the energy accumulated in the outer shell is absorbed by the remaining solid PCM after the end of the exposure, which would be in line with the continuous increase in temperature for higher times (Figure 15a, 30 s < t < 60 s). To show that this is the case, consider Figure 16a. It shows the temperature profiles along the garment–skin system for T_m = 200 ºC, for case A1. As can be seen, in the region 0.0007 m < x < 0.0017 m (where the PCM is located), after the exposure (t > 8 s), there is still PCM in the temperature range between T_s and T_l (190 ºC and 210 ºC in this case, respectively), that is, in the solid phase. To show this more clearly consider Figure 17. It shows the percentage of PCM latent heat usage relative to the total available, that is, the PCM melted compared to that available in the system. As shown in Figure 17a for T_m = 200 ºC, only 40 % of the PCM melts during the exposure (t < 8 s). Part of the PCM is then used to absorb the heat accumulated in the outer shell after the exposure (8 s < t < 10 s between 0 m < x < 0.0017 m in Figure 16a, and 8 s < t < 20 s in Figure 17a for T_m = 200 ºC). After the absorption of heat still only 65% of the PCM has melted (T_m = 200 ºC, t = 17 s in Figure 17a). This means that more energy is transferred towards the skin in comparison to other PCM melting temperatures (Figure 16b) which allow for a greater percentage of PCM melted during the process (Figure 17a). Once the temperature of the PCM approaches 200 ºC (melting temperature), and after the exposure and the absorption of the remaining heat accumulated in the clothing layers (which cause the steep temperature gradients), the solidification of the PCM takes place (t > 20 s in

Figure 17a) causing a release of latent heat into the garment–skin system (10 s < t < 30 s in Figure 16a). Hence, the higher the melting temperature, the less heat absorbed as latent heat, and the earlier its release. Similar phenomena happen for Case A3. In Case A2 however, since all of the PCM melts independently of the melting temperature considered (Figure 17b), what essentially determines whether or not a melting temperature is adequate is at what time the phase change takes place in the process. This will be further discussed when the thermal performance (t_{44} and t_{55}) is analysed.

Another interesting thing observed in Case A2 is that for a higher T_m, the solidification process is faster (t > 300 s, Figure 17b, evidenced by decreasing slopes with increasing T_m). This also happens for the other cases, but because the PCM melts less with increasing T_m, the effect is not so visible. This has naturally to do with the simple fact that latent heat released at a higher T_m implies a greater heat transfer because of a higher temperature gradient between the PCM and the skin (e.g. Figure 16a).

Figure 18 shows the total energy stored during the process, in the PCM (see Annex D for details on calculation). As shown, an increase in T_m origins a decrease in the heat accumulated in the PCM (Figure 18). This is consistent with the evidence discussed above that more heat is transferred towards the skin (Figure 16b) as less is accumulated in the PCM (Figure 18) with increasing T_m. A lower storage of energy in the PCM means that the energy is accumulated in the garment layers which have a singificantly less thermal inertia. Thus higher temperatures will be developed throughout the garments which will result in a higher heat transfer to the skin.

Figure 19a shows the exposure times for first and second degree burns (t_{44} and t_{55}) with respect to the PCM melting temperature. The relative exposure times are shown in Figure 19b. As expected, an increase in T_m originates a decrease in t_{44} and t_{55} (i.e. burns happen faster), for all cases (Figure 19a). This decrease is sudden and happens in a specific range of melting temperatures (e.g. 140 ºC < T_m < 200 ºC, *Case A1_τ55*, Figure 19b). For most cases, this change happens for t_{44}, at lower T_m than for t_{55} (Figure 19b). For case A1, when T_m = 200 ºC, the phase change happens later and not all of the PCM melts during the exposure, thus not making full use of the available latent heat (0.0007 m < x < 0.0017 m in Figure 16a, and T_m = 200 ºC in Figure 17a). But for a lower T_m, the PCM melts completely during the exposure thus decreasing the heat transferred towards the skin (e.g. Figure 17a). A low T_m implies that a phase change happens early enough

in the process so that most of the PCM melts before the epidermis/dermis boundary reaches 44 ºC. This means that most heat that goes in the garment-skin system at initial times, before the epidermis/dermis reaches 44 ºC, is stored as latent and not sensible heat. This can be clearly seen from Figure 17 where for initial times, higher T_m make the PCM melt less or later. However, for Case A1, this tendency is inverted (τ_{44} starts decreasing before τ_{55} as shown in Figure 19b). This is because by the time the epidermis/dermis layer reaches 55 ºC, the PCM is already solidifying when T_m is higher than 150 ºC (T_m = 150 ºC, 30 s < t < 50 s in Figure 15a and Figure 17a).

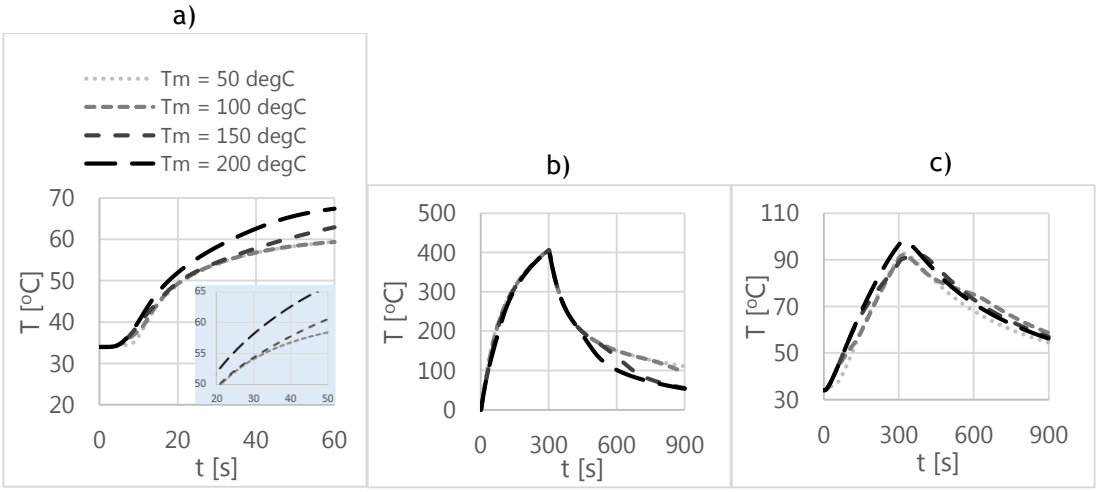

Figure 15: Temperature histories obtained at Epidermis/Dermis boundary for cases: a) A1 (84 kW/m² for 8 s); b) Case A2 (12 kW/m² for 5 min) c); Case A3 (5 kW/m² for 5 min)

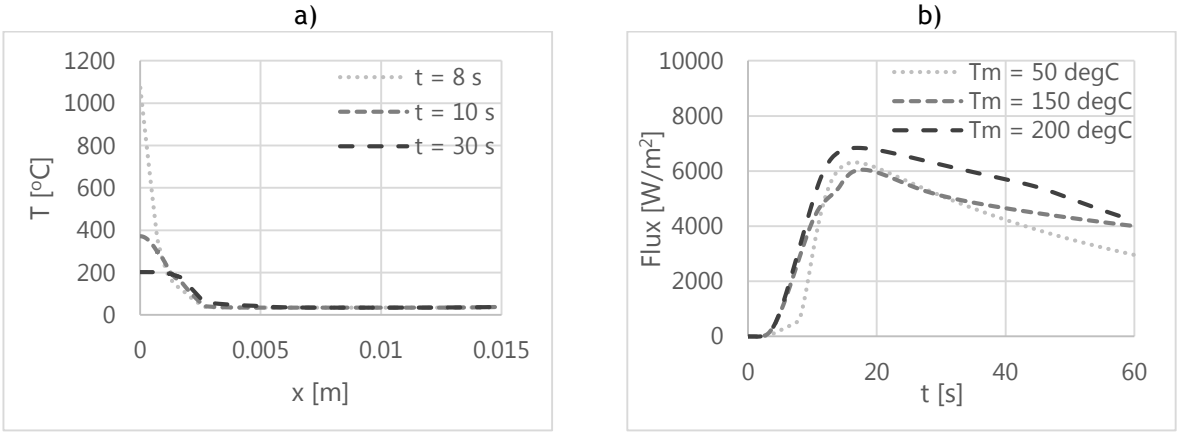

Figure 16: a) Temperature profiles obtained for Case A1 and T_m = 200 ºC; b); Heat flux histories at Epidermis/ Dermis layer obtained for Tm = 50 ºC, 150 ºC and 200 ºC.

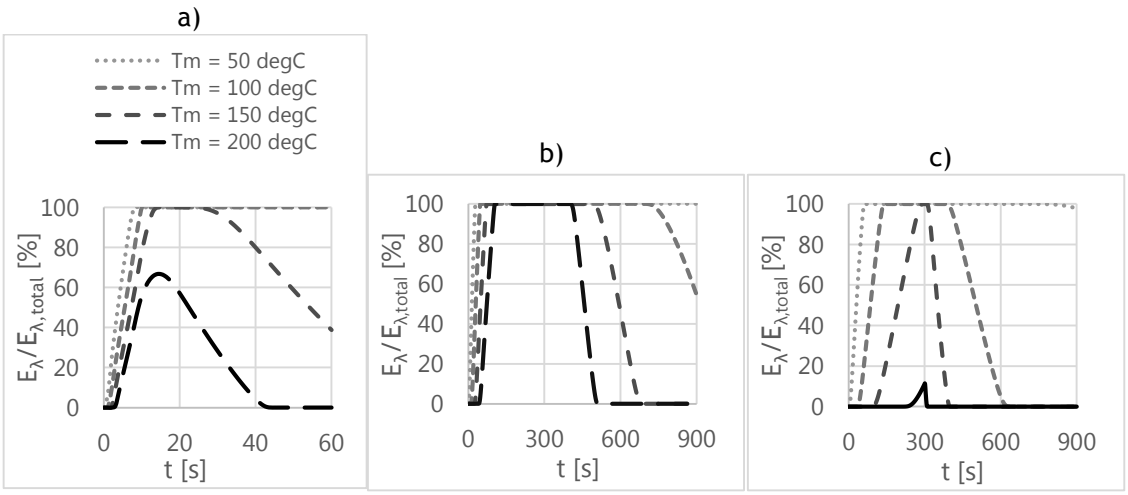

Figure 17: Latent energy accumulated in PCM domain in terms of percentage relative to total latent heat available ($E_{\lambda,total}$ = mλ) for cases; a) A1 (84 kW/m² for 8 s); b) A2 (12 kW/m² for 5 min); c) A3 (5 kW/m² for 5 min)

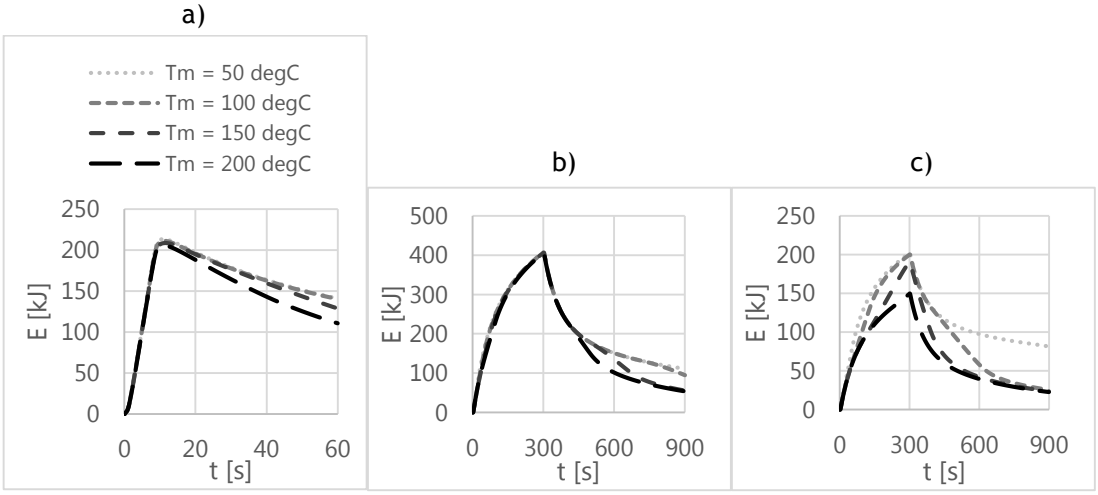

Figure 18: Total energy accumulated in PCM domain for cases: a) A1 (84 kW/m^2 for 8 s); b) Case A2 (12 kW/m^2 for 5 min); c) Case A3 (5 kW/m^2 for 5 min)

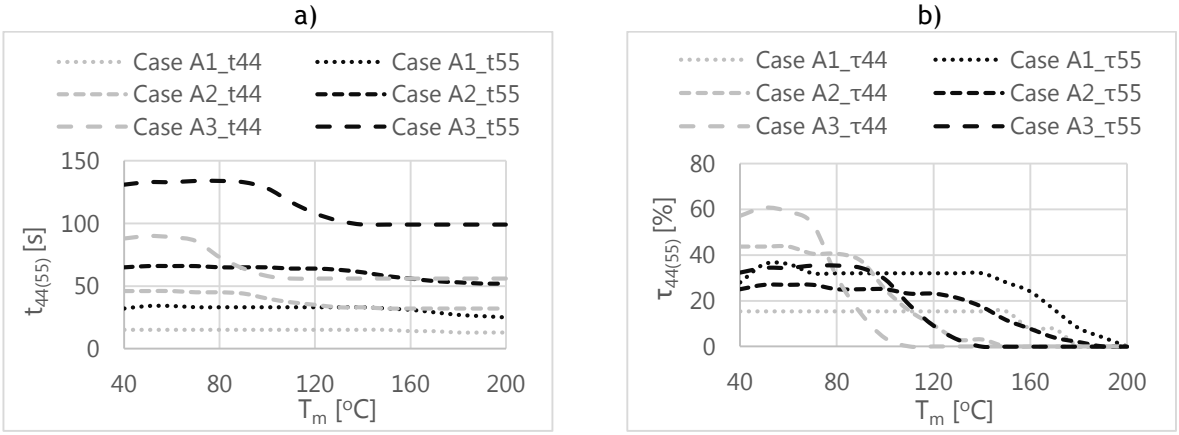

Figure 19: Absolute and relative time to first (t_{44} and τ_{44}, respectively) and second (t_{55} and τ_{55}, respectively) degree burns at the skin; a) Absolute time to burns b) relative time to burns

3.4 Influence of PCM layer position

As stated before, a PCM layer can be interpreted as a layer having a thermal inertia varying with temperature. During a charge process (exposure to heat, causing melting), such as the one at stake in this current study, the PCM layer has a variable thermal inertia throughout the process (Annex Figure 1). In the charge process, if the PCM changes phase, it offers a singificantly higher thermal inertia to their system as compared to the other garment layers.

A layer that has a high thermal inertia associated to it is, in principle, to be put near the heat source as it promotes lower temperatures in the garment-skin system (Phelps et al., 2014). This is valid, if the intention is to minimize heat transfer (with time) towards the system. This concept represents, in a way, the function of a PCM in the context of a firefighter garment.

Simulations were run with various PCM configurations (See Annex C, for PCM configurations chosen in the simulations) with increasing distances between the PCM layer and the environment (thus with PCM layers placed closer to the skin). For each configuration, temperature histories at the epidermis/dermis boundary were obtained (Figure 20). Also heat fluxes reaching the epidermis/dermis boundary were calculated (Figure 21). Temperature profiles were computed, however here shown is just for Case A1 (Figure 22). Parameters t_{44} and t_{55} were obtained along with the relative times (Figure 23). Total accumulated energy in the PCM domain was obtained during the process for the different configurations (Figure 24) along with the PCM melting percentage (Figure 25). A spatial co-ordinate *d* was defined according to Annex Figure 2. So, when d = 0 mm, the PCM layer is between the outer shell and thermal inner. When d = 0.95 mm, the PCM layer is between the thermal inner and the epidermis.

As can be seen, a configuration of the PCM more towards the skin (d > 0 mm) originates an increase in the temperatures obtained at the epidermis/dermis layer (Figure 20) coupled with an increase in the delay of the melting of the PCM (Figure 25). This is in direct compliance with the total energy accumulated at the PCM, where a lower *d* (PCM closer to the environment) originates a higher energy accumulation (Figure 24). This happens for all cases. It can be concluded that shifting the PCM layer towards the skin makes the PCM change phase at a later stage in the process. However the PCM

completely melts for all the configurations and exposure scenarios considered (Figure 25).

This translates into a higher time to burns (t_{44} and t_{55}) when the PCM layer is located closer to the environment and further from the skin (lower values of *d*, Figure 23). Note that, in Figure 23b, for Case A1, τ_{55} has the biggest relative variation with the PCM position considered. As *d* increases (PCM layer closer to the skin), steeper temperature profiles throughout the garment system are obtained (Figure 22). This in turn implies greater heat fluxes reaching the skin for increasing *d* at higher times, since the steep temperature gradients are initially located mostly in outer positions (0 m < ***x*** < 0.003 m, Figure 22 and Figure 21a, 20 s < *t* < 40 s). These fluxes vary dramatically with PCM layer position (*d*), and such variations happen at times where the epidermis/dermis layer reaches 55 ºC (Figure 21a and Figure 20a, 20 s < *t* < 40 s). To note that also with increasing *d*, the phase change can take place after the exposure (*t* > 8 s, Figure 25a). This phenomena is similar to the one observed in section 3.3. Hence changing the position of the PCM layer has effect in the time the phase change takes place in this context. Being the layer with the highest thermal inertia (PCM), a higher *d* (positioned more towards the skin) implies that, the other garment layers with lower thermal inertia are positioned closer to the environment, which will translate to the obtainance of higher temperatures throughout the garment–skin system (e.g. Figure 22) so more heat reaches the skin (Figure 21), and hence higher temperatures at the epidermis/dermis boundary are obtained (Figure 20). This happens for all cases.

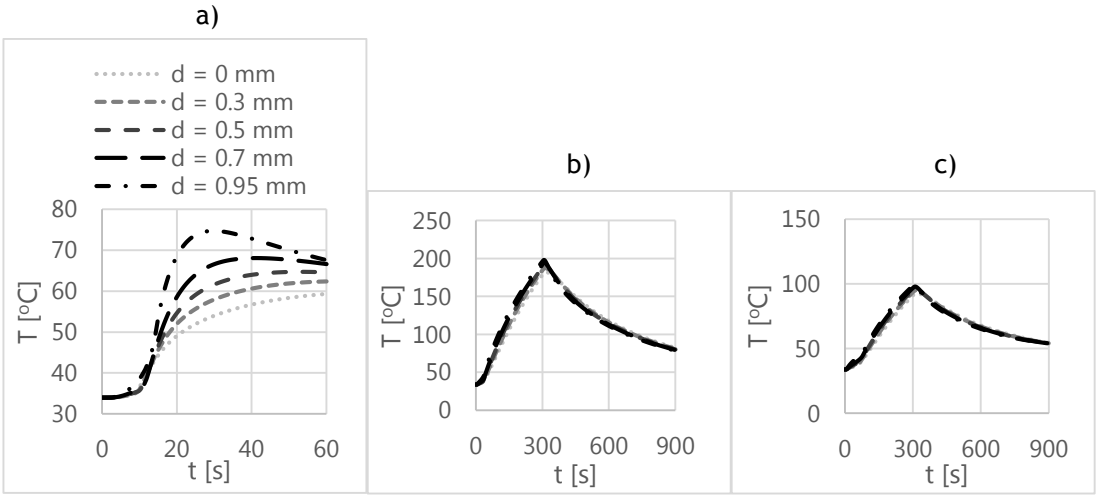

Figure 20: Temperature histories obtained at Epidermis/Dermis boundary for cases: a) A1 (84 kW/m² for 8 s); b) Case A2 (12 kW/m² for 5 min); c) Case A3 (5 kW/m² for 5 min)

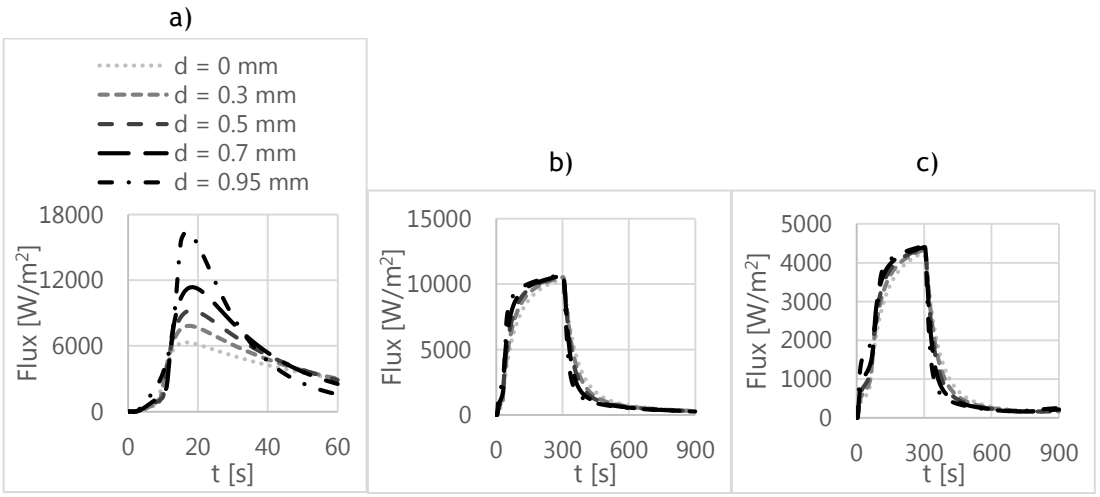

Figure 21: Heat flux at epidermis/dermis boundary: a) Case A1 (84 kW/m^2 for 8 s); b) Case A2 (12 kW/m^2 for 5 min); c) Case A3 (5 kW/m^2 for 5 min)

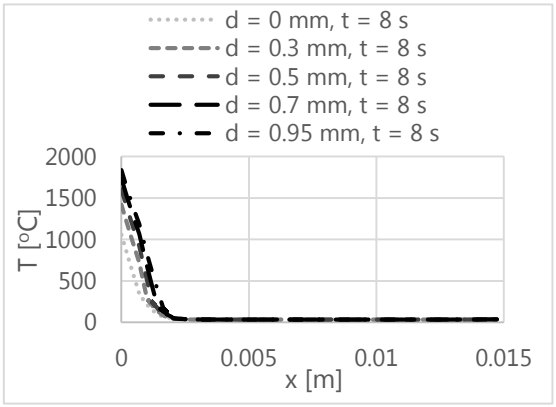

Figure 22: Temperature profiles for Case A1 (84 kW/m^2 for 8 s) for the indicated PCM layer positions (*d*) at *t* = 8 s.

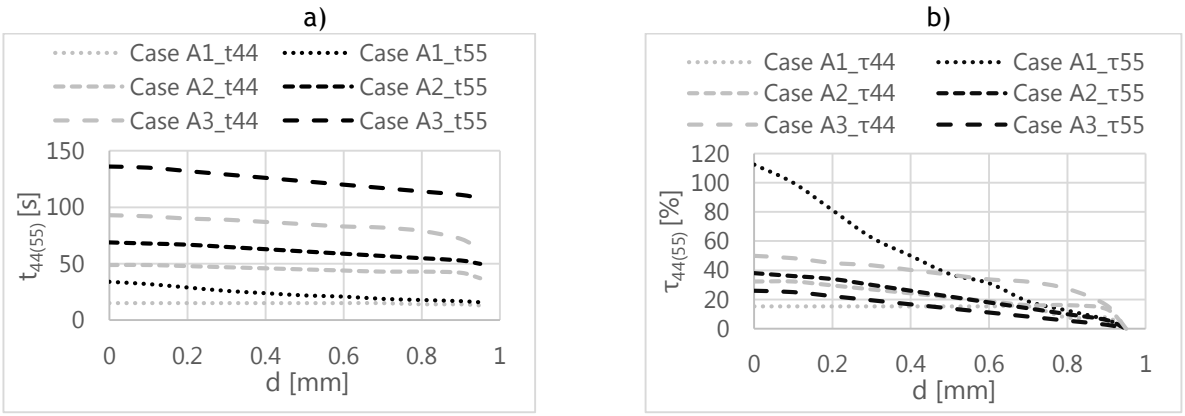

Figure 23: Absolute and relative time to first (t_{44} and τ_{44}, respectively) and second (t_{55} and τ_{55}, respectively) degree burns at the skin; a) Absolute time to burns b) relative time to burns

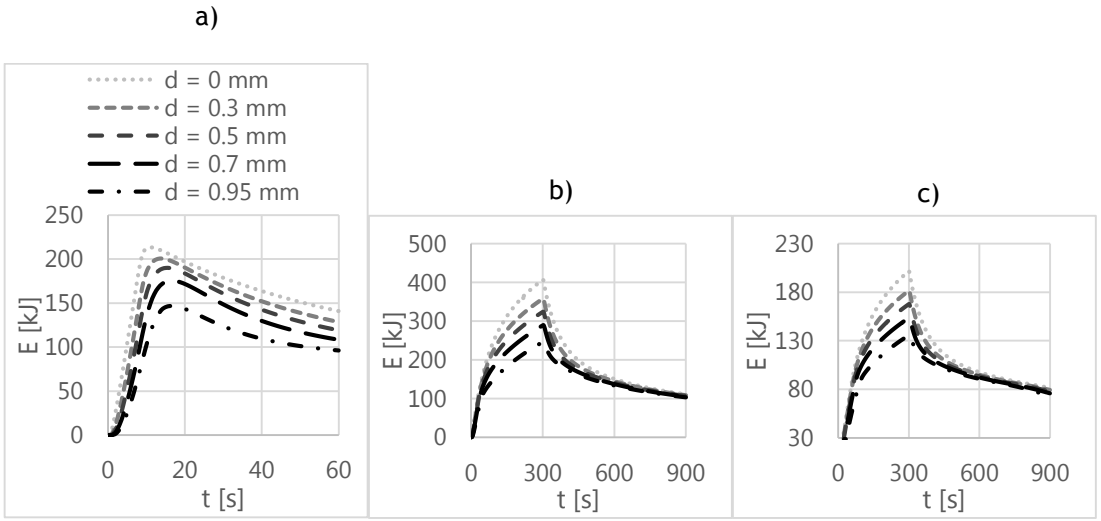

Figure 24: Total energy accumulated in PCM domain for cases: a) A1 (84 kW/m^2 for 8 s); b) Case A2 (12 kW/m^2 for 5 min); c) Case A3 (5 kW/m^2 for 5 min)

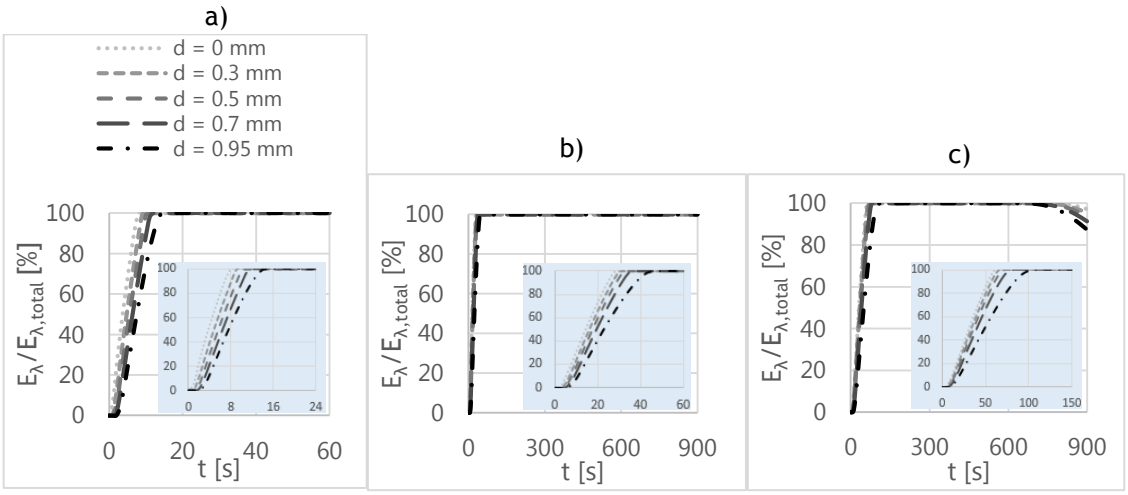

Figure 25: Latent energy accumulated in PCM domain in terms of percentage relative to total latent heat available ($E_{\lambda,total}$ = mλ) for cases: a) A1 (84 kW/m² for 8 s); b) A2 (12 kW/m² for 5 min); c) A3 (5 kW/m² for 5 min)

4. Conclusion

The four main variables influencing the thermal performance of a PCM layer incorporated in a latent heat thermal enegy storage system (LHTES), more precisely in a firefighting protective clothing assembly (FFPC), were subject to study. PCMs contribute indeed to an enhancement in the thermal performance of a FFPC by absorbing part of the incoming heat flux in the form of latent heat. As a result of the parametric study done, the following conclusions can be drawn;

i.) A higher latent heat, implies that more of the incoming heat flux is absorbed as latent heat. Hence the available latent heat should be as big as possible. For the exposure Case A1 (84 kW/m^2 for 8 s) the effect of latent heat was found to be the greatest in preventing the skin from reaching a second-degree burn (i.e. reaching 55 ^{o}C). This had to do with solid PCM still being present after the exposure.

ii.) Mass was found to have a similar effect to latent heat. A higher mass not only increases the thermal resistance associated to the PCM layer (higher thickness), but it also increases the total latent heat available. Again, if solid PCM is present after a heat exposure, the thermal performance increases significantly. The accumulated heat present after an exposure is indeed associated with high temperatures in the garment-skin system. Absorbing this heat in the latent form stores it at a controlled temperature level (T_m), reducing the temperatures in the garment–skin system.

iii.) The optimum position of the PCM layer was found to be closest to the environment and furthest from the skin (i.e. d = 0 mm). This hinders the development of higher temperatures in the garment-skin system since the high intertia associated with the PCM layer is used more effectively. PCM layer position was found to have its greatest influence in exposure Case A1 (84 kW/m^2 for 8 s), due to PCM solid still being present after the exposure, which can absorb the energy already inside the clothing system.

iv.) The melting temperature of the PCM should be high enough so its melting does not commence before the exposure, but also low enough to promote its melting. For exposure Case A1 (84 kW/m^2 for 8 s), a melting temperature in the range 50 ^{o}C < T_m < 140 ^{o}C is considered adequate whilst for exposure Cases A2 and A3 (12 kW/m^2 and 5 kW/m^2 for 5 min, respectively) melting temperatures in the ranges of 50 ^{o}C < T_m < 90 ^{o}C and 50 ^{o}C < T_m < 70 ^{o}C originate similar thermal performance, respectively. To note that these conclusions are taken if the objective is to increase the time for the skin to reach 44 ^{o}C and 55 ^{o}C.

The variables that were found to have greatest influence on thermal performance were PCM mass and latent heat followed by its melting temperature and position. This was to be expected since under such high intensity exposures, temperature gradients develop very rapidly and so the transient response is majorly influenced by the latent energy present.

5. Bibliography

Agyenim, F., Hewitt, N., Eames, P., & Smyth, M. (2010). A review of materials, heat transfer and phase change problem formulation for latent heat thermal energy storage systems (LHTESS). *Renewable and Sustainable Energy Reviews*, *14*(2), 615–628. http://doi.org/10.1016/j.rser.2009.10.015

Al-Hamadani, a. a. F., & Shukla, S. K. (2012). Water Distillation Using Solar Energy System with Lauric Acid as Storage Medium. *International Journal of Energy Engineering*, *1*(1), 1–8. http://doi.org/10.5923/j.ijee.20110101.01

Al-Hamadani, A. A. F., & Shukla, S. K. (2012). Water Distillation Using Solar Energy System with Lauric Acid as Storage Medium. *International Journal of Energy Engineering*, *1*(1), 1–8. http://doi.org/10.5923/j.ijee.20110101.01

Barr, D., Gregson, W., & Reilly, T. (2010). The thermal ergonomics of firefighting reviewed. *Applied Ergonomics*, *41*(1), 161–172. http://doi.org/10.1016/j.apergo.2009.07.001

Bühler, M., Popa, a. M., Scherer, L. J., Lehmeier, F. K. S., & Rossi, R. M. (2013). Heat protection by different phase change materials. *Applied Thermal Engineering*, *54*(2), 359–364. http://doi.org/10.1016/j.applthermaleng.2013.02.025

Comsol. (2011). *Heat Transfer Module: User's Guide*.

Dutil, Y., Rousse, D. R., Salah, N. Ben, Lassue, S., & Zalewski, L. (2011). A review on phase-change materials: Mathematical modeling and simulations. *Renewable and Sustainable Energy Reviews*, *15*(1), 112–130. http://doi.org/10.1016/j.rser.2010.06.011

Farid, M. M., Khudhair, A. M., Razack, S. A. K., & Al-Hallaj, S. (2004). A review on phase change energy storage: Materials and applications. *Energy Conversion and Management*, *45*, 1597–1615. http://doi.org/10.1016/j.enconman.2003.09.015

Gao, C., Kuklane, K., & Holmér, I. (2010). Cooling vests with phase change material packs: the effects of temperature gradient, mass and covering area. *Ergonomics*, *53*(5), 716–23. http://doi.org/10.1080/00140130903581649

House, J. R., Lunt, H. C., Taylor, R., Milligan, G., Lyons, J. a, & House, C. M. (2013). The impact of a phase-change cooling vest on heat strain and the effect of different cooling pack melting temperatures. *European Journal of Applied Physiology*, *113*(5), 1223–31. http://doi.org/10.1007/s00421-012-2534-2

Hsiao, H., Whitestone, J., Kau, T. Y., Whisler, R., Routley, J. G., & Wilbur, M. (2014). Sizing firefighters: Method and implications. *Human Factors*, *56*(5), 873–910. http://doi.org/10.1177/0018720813516359

Hu, H., & Argyropoulos, S. a. (1999). Mathematical modelling of solidification and

melting: a review. *Modelling and Simulation in Materials Science and Engineering*, *4*, 371–396. http://doi.org/10.1088/0965-0393/4/4/004

Hu, Y., Huang, D., Qi, Z., He, S., Yang, H., & Zhang, H. (2012). Modeling thermal insulation of firefighting protective clothing embedded with phase change material. *Heat and Mass Transfer*, *49*(4), 567–573. http://doi.org/10.1007/s00231-012-1103-x

Hunag, D., Li, Y., Tong, L., Yang, H., & Zhang, H. (2010). Modeling Heat Transfer in Phase Change Material Bedded Firefighting Protective Clothing under Fire Exposure. In *Progress in safety science and technology* (Vol. VIII, pp. 921–926). SCIENCE PRESS BEIJING, 16 DONGHUANGCHENGGEN NORTH ST, BEIJING 100707, PEOPLES R CHINA.

McCarthy, L. K., & Marzo, M. (2012). The Application of Phase Change Material in Fire Fighter Protective Clothing. *Fire Technology*, *48*(4), 841–864. http://doi.org/10.1007/s10694-011-0248-3

Mercer, G. N., & Sidhu, H. S. (2008). Mathematical modelling of the effect of fire exposure on a new type of protective clothing. *Anziam J.*, *49*, 289–305.

Mercer, G. N., & Sidhu, H. S. (2009). A Theoretical Investigation into Phase Change Clothing Benefits for Firefighters under Extreme Conditions. *Chemical Product and Process Modeling*, *4*(3). http://doi.org/10.2202/1934-2659.1349

Nybo, L., Secher, N. H., & Nielsen, B. (2002). Inadequate heat release from the human brain during prolonged exercise with hyperthermia. *The Journal of Physiology*, *545*(2), 697–704. http://doi.org/10.1113/jphysiol.2002.030023

Pause, B. (2010). *Phase change materials and their application in coatings and laminates for textiles. Smart Textile Coatings and Laminates*. Woodhead Publishing Limited. http://doi.org/http://dx.doi.org/10.1533/9781845697785.2.236

Phelps, H., & Sidhu, H. (2015). A mathematical model for heat transfer in fire fighting suits containing phase change materials. *Fire Safety Journal*, *74*, 43–47. http://doi.org/10.1016/j.firesaf.2015.04.007

Phelps, H., Sidhu, H., & Sidhu, L. (2014). Modelling heat transport in protective fire fighting clothing containing phase change materials. Retrieved from http://www.icheme.org/chemeca2014/program/papers.aspx

Pielichowska, K., & Pielichowski, K. (2014). Phase change materials for thermal energy storage. *Progress in Materials Science*, *65*(0), 67–123. http://doi.org/http://dx.doi.org/10.1016/j.pmatsci.2014.03.005

Rossi, R., & Bolli, W. (2005). Phase change materials for improvement of heat protection. *Advanced Engineering Materials*, *7*(5), 368–373.

http://doi.org/10.1002/adem.200500064

Sharma, A., Tyagi, V. V., Chen, C. R., & Buddhi, D. (2009). Review on thermal energy storage with phase change materials and applications. *Renewable and Sustainable Energy Reviews*, *13*, 318–345. http://doi.org/10.1016/j.rser.2007.10.005

Shim, H., McCullough, E. a., & Jones, B. W. (2001). Using Phase Change Materials in Clothing. *Textile Research Journal*, *71*(6), 495–502. http://doi.org/10.1177/004051750107100605

Solomon, A. D., & Alexiades, V. (1993). Problem Formulation. In *Mathematical Modelling of Melting and Freezing Processes* (pp. 1–32). Hemisphere Publishing Corporation.

Tu, J., Yeoh, G. H., & Liu, C. (2008). *Computational Fluid Dynamics a Practical Approach*.

Tyagi, V., & Buddhi, D. (2007). PCM thermal storage in buildings: A state of art. *Renewable and Sustainable Energy Reviews*, *11*(6), 1146–1166. http://doi.org/10.1016/j.rser.2005.10.002

Voller, V. R., Swaminathan, C. R., & Thomas, B. G. (1990). Fixed grid techniques for phase change problems: A review. *International Journal for Numerical Methods in Engineering*, *30*(4), 875–898. http://doi.org/10.1002/nme.1620300419

Wilkes, J. O. (2009). *Introduction to COMSOL Multiphysics*. Retrieved from http://cdn.comsol.com/documentation/5.1.0.145/IntroductionToCOMSOLMultiphysics.pdf

Zalba, B. (2003). Review on thermal energy storage with phase change: materials, heat transfer analysis and applications. *Applied Thermal Engineering*, *23*(3), 251–283. http://doi.org/10.1016/S1359-4311(02)00192-8

Zhu, F., Feng, Q., Liu, R., & Yu, B. (2015). Enhancing the Thermal Protective Performance of Firefighters ' Protective Fabrics by Incorporating Phase Change Materials, *2*(110), 68–73.

6. Annexes

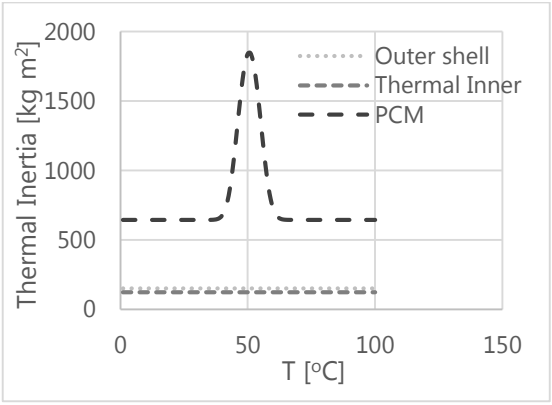

Annex figure 1: Thermal inertia of the various indicated layers with respect to temperature.

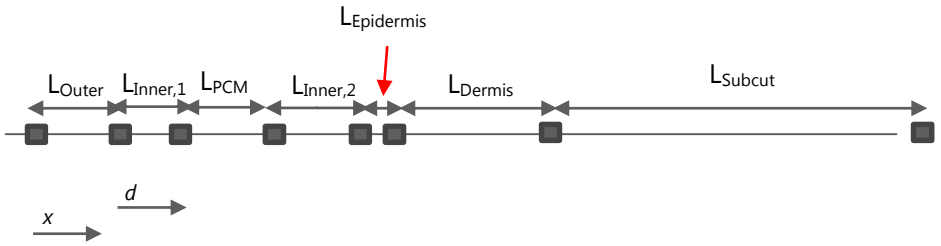

Annex figure 2: Schematic diagram showing PCM layer laminated inside thermal inner (diagram not to scale). The *d* coordinate represents the distance the PCM layer is located relative to the position where the PCM layer is between the thermal inner and the outer shell. Note that for all cases $L_{inner,1}+L_{inner,2}$ = 0.95 mm

Annex A: Materials and properties

Table 3: Properties of the materials of the various garment-skin layers

Property	Outer	PCM	Inner	Epidermis	Dermis	Subcut
ρ [kg/m^3]	286	862	220	1200	1200	1000
C [J/(kg·K)]	1005	--	1300	3600	3300	2500
k [W/(m·K)]	0.08	0.16	0.052	0.24	0.45	0.18
width [mm]	0.7	1.0	0.95	0.080	2.0	10.0
G [1/s]					0.00125	0.00125

Where ρ is the density in kg/m^3, C the specific heat in J/(kg·K), k the thermal conductivity in W/(m·K), and G the blood perfusion rate in s^{-1}. Blood properties were taken from (Nybo et al., 2002).

Annex B: Meshes

Some of the domains contained distributed Meshes. Domain a_1 contained a geometric distribution Mesh in a reverse order. The steep gradients developed in domain a_2 when the PCM starts changing phase, could lead to difficulties in the connectivity between the Meshes in domains a_1 and a_2 . As the PCM changes phase, the temperature gradients developed become less steep. Fewer elements are required for higher positions, hence the distribution imposed in the Mesh in domain a_2.

Table 4: Meshes used in study case

Domain	Properties	Mesh
α_1	• Elements • Distribution type/ratio	50 Reverse geometric/10
α_2		500 Arithmetic/50
α_3		50 --
α_4		50 --
β_1		50 --
β_2		50 --
β_3		50 --

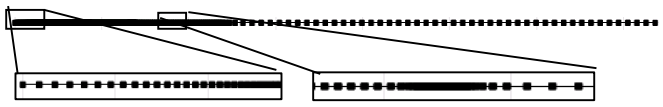

Annex Figure 3: Mesh used for all simulations (Figure 1 shows more details on the respective geometry)

Annex C: Simulated cases

Table 5: Simulated values of parameters for each of the respective cases shown

Cases	d [mm]	T_m [°C]	λ [kJ/kg]	m [g]	L_{PCM} [mm]	$E_{\lambda,total}$ [kJ]	t_{44} [s]	t_{55} [s]	Imbalances [%]	ΔT_{mushy} [°C]
Case A1_d_0	0	50.6	199.6	307	1	61.3	15	34	0.000644	20
Case A1_d_0.1	0.1	50.6	199.6	307	1	61.3	15	32	0.001403	20
Case A1_d_0.2	0.2	50.6	199.6	307	1	61.3	15	29	0.001189	20
Case A1_d_0.3	0.3	50.6	199.6	307	1	61.3	15	26	0.000994	20
Case A1_d_0.4	0.4	50.6	199.6	307	1	61.3	15	24	0.000707	20
Case A1_d_0.5	0.5	50.6	199.6	307	1	61.3	15	22	0.001718	20
Case A1_d_0.6	0.6	50.6	199.6	307	1	61.3	15	21	0.000747	20
Case A1_d_0.7	0.7	50.6	199.6	307	1	61.3	15	19	0.001080	20
Case A1_d_0.8	0.8	50.6	199.6	307	1	61.3	14	18	0.001007	20
Case A1_d_0.9	0.9	50.6	199.6	307	1	61.3	14	17	0.000927	20
Case A1_d_0.95	0.95	50.6	199.6	307	1	61.3	13	16	0.000677	20
Case A2_d_0	0	50.6	199.6	307	1	61.3	49	69	0.001158	20
Case A2_d_0.1	0.1	50.6	199.6	307	1	61.3	49	68	0.001231	20
Case A2_d_0.2	0.2	50.6	199.6	307	1	61.3	48	67	0.001020	20
Case A2_d_0.3	0.3	50.6	199.6	307	1	61.3	47	65	0.001145	20
Case A2_d_0.4	0.4	50.6	199.6	307	1	61.3	46	63	0.000999	20
Case A2_d_0.5	0.5	50.6	199.6	307	1	61.3	45	61	0.001037	20
Case A2_d_0.6	0.6	50.6	199.6	307	1	61.3	44	59	0.001213	20
Case A2_d_0.7	0.7	50.6	199.6	307	1	61.3	43	57	0.001224	20
Case A2_d_0.8	0.8	50.6	199.6	307	1	61.3	43	55	0.001051	20
Case A2_d_0.9	0.9	50.6	199.6	307	1	61.3	42	53	0.000951	20
Case A2_d_0.95	0.95	50.6	199.6	307	1	61.3	37	50	0.000901	20
Case A3_d_0	0	50.6	199.6	307	1	61.3	93	136	0.002574	20
Case A3_d_0.1	0.1	50.6	199.6	307	1	61.3	92	135	0.002755	20
Case A3_d_0.2	0.2	50.6	199.6	307	1	61.3	91	132	0.002483	20
Case A3_d_0.3	0.3	50.6	199.6	307	1	61.3	89	129	0.002420	20
Case A3_d_0.4	0.4	50.6	199.6	307	1	61.3	87	126	0.002466	20

Cases	d [mm]	T_m [°C]	λ [kJ/kg]	m [g]	L_{PCM} [mm]	$E_{\lambda,total}$ [kJ]	t_{44} [s]	t_{55} [s]	Imbalances [%]	ΔT_{mushy} [°C]
Case A3_d_0.5	0.5	50.6	199.6	307	1	61.3	85	123	0.002093	20
Case A3_d_0.6	0.6	50.6	199.6	307	1	61.3	83	120	0.002143	20
Case A3_d_0.7	0.7	50.6	199.6	307	1	61.3	82	117	0.001966	20
Case A3_d_0.8	0.8	50.6	199.6	307	1	61.3	79	114	0.001943	20
Case A3_d_0.9	0.9	50.6	199.6	307	1	61.3	72	111	0.001678	20
Case A3_d_0.95	0.95	50.6	199.6	307	1	61.3	62	108	0.001539	20
Case A1_Tm_40	0	40	199.6	307	1	61.3	15	32	0.001319	20
Case A1_Tm_50	0	50	199.6	307	1	61.3	15	34	0.000801	20
Case A1_Tm_60	0	60	199.6	307	1	61.3	15	34	0.001802	20
Case A1_Tm_70	0	70	199.6	307	1	61.3	15	33	0.000706	20
Case A1_Tm_80	0	80	199.6	307	1	61.3	15	33	0.00137	20
Case A1_Tm_90	0	90	199.6	307	1	61.3	15	33	0.000552	20
Case A1_Tm_100	0	100	199.6	307	1	61.3	15	33	0.000626	20
Case A1_Tm_110	0	110	199.6	307	1	61.3	15	33	0.000649	20
Case A1_Tm_120	0	120	199.6	307	1	61.3	15	33	0.000839	20
Case A1_Tm_130	0	130	199.6	307	1	61.3	15	33	0.000923	20
Case A1_Tm_140	0	140	199.6	307	1	61.3	15	33	0.001292	20
Case A1_Tm_150	0	150	199.6	307	1	61.3	15	32	0.001183	20
Case A1_Tm_160	0	160	199.6	307	1	61.3	14	31	0.001099	20
Case A1_Tm_170	0	170	199.6	307	1	61.3	14	29	0.000981	20
Case A1_Tm_180	0	180	199.6	307	1	61.3	13	27	0.001222	20
Case A1_Tm_190	0	190	199.6	307	1	61.3	13	26	0.001306	20
Case A1_Tm_200	0	200	199.6	307	1	61.3	13	25	0.0014	20
Case A2_Tm_40	0	40	199.6	307	1	61.3	49	68	0.00094	20
Case A2_Tm_50	0	50	199.6	307	1	61.3	49	69	0.001368	20
Case A2_Tm_60	0	60	199.6	307	1	61.3	49	69	0.001286	20
Case A2_Tm_70	0	70	199.6	307	1	61.3	48	69	0.001038	20
Case A2_Tm_80	0	80	199.6	307	1	61.3	48	68	0.001202	20
Case A2_Tm_90	0	90	199.6	307	1	61.3	47	68	0.001135	20
Case A2_Tm_100	0	100	199.6	307	1	61.3	43	68	0.00128	20

Cases	d [mm]	T_m [°C]	λ [kJ/kg]	m [g]	L_{PCM} [mm]	$E_{\lambda,total}$ [kJ]	t_{44} [s]	t_{55} [s]	Imbalances [%]	ΔT_{mushy} [°C]
Case A2_Tm_110	0	110	199.6	307	1	61.3	40	67	0.001226	20
Case A2_Tm_120	0	120	199.6	307	1	61.3	38	67	0.001245	20
Case A2_Tm_130	0	130	199.6	307	1	61.3	36	66	0.001314	20
Case A2_Tm_140	0	140	199.6	307	1	61.3	36	64	0.001223	20
Case A2_Tm_150	0	150	199.6	307	1	61.3	35	61	0.001134	20
Case A2_Tm_160	0	160	199.6	307	1	61.3	35	59	0.001451	20
Case A2_Tm_170	0	170	199.6	307	1	61.3	35	57	0.001212	20
Case A2_Tm_180	0	180	199.6	307	1	61.3	35	56	0.001224	20
Case A2_Tm_190	0	190	199.6	307	1	61.3	35	55	0.001267	20
Case A2_Tm_200	0	200	199.6	307	1	61.3	35	55	0.001478	20
Case A3_Tm_40	0	40	199.6	307	1	61.3	91	134	0.002355	20
Case A3_Tm_50	0	50	199.6	307	1	61.3	93	136	0.002478	20
Case A3_Tm_60	0	60	199.6	307	1	61.3	92	136	0.002504	20
Case A3_Tm_70	0	70	199.6	307	1	61.3	89	137	0.002389	20
Case A3_Tm_80	0	80	199.6	307	1	61.3	76	137	0.002262	20
Case A3_Tm_90	0	90	199.6	307	1	61.3	67	136	0.002544	20
Case A3_Tm_100	0	100	199.6	307	1	61.3	61	131	0.002091	20
Case A3_Tm_110	0	110	199.6	307	1	61.3	59	120	0.002103	20
Case A3_Tm_120	0	120	199.6	307	1	61.3	59	111	0.002032	20
Case A3_Tm_130	0	130	199.6	307	1	61.3	59	105	0.002153	20
Case A3_Tm_140	0	140	199.6	307	1	61.3	59	102	0.002289	20
Case A3_Tm_150	0	150	199.6	307	1	61.3	59	102	0.002239	20
Case A3_Tm_160	0	160	199.6	307	1	61.3	59	102	0.001966	20
Case A3_Tm_170	0	170	199.6	307	1	61.3	59	102	0.001897	20
Case A3_Tm_180	0	180	199.6	307	1	61.3	59	102	0.001843	20
Case A3_Tm_190	0	190	199.6	307	1	61.3	59	102	0.001563	20
Case A3_Tm_200	0	200	199.6	307	1	61.3	59	102	0.001048	20
Case A1_m_200	0	50.6	199.6	200	0.65	39.9	10	15	0.000536	20
Case A1_m_400	0	50.6	199.6	400	1.30	79.8	23	>18	0.000931	20
Case A1_m_600	0	50.6	199.6	600	1.95	119.76	67	>18	0.001055	20

Cases	d [mm]	T_m [°C]	λ [kJ/kg]	m [g]	L_{PCM} [mm]	$E_{\lambda,total}$ [kJ]	t_{44} [s]	t_{55} [s]	Imbalances [%]	ΔT_{mushy} [°C]
Case A1_m_800	0	50.6	199.6	800	2.60	159.68	>18	>18	0.000978	20
Case A1_m_1000	0	50.6	199.6	1000	3.26	199.6	>18	>18	0.001101	20
Case A1_m_1200	0	50.6	199.6	1200	3.91	239.52	>18	>18	0.001070	20
Case A1_m_1400	0	50.6	199.6	1400	4.56	279.44	>18	>18	0.001220	20
Case A1_m_1600	0	50.6	199.6	1600	5.21	319.36	>18	>18	0.001184	20
Case A1_m_1800	0	50.6	199.6	1800	5.86	359.28	>18	>18	0.001370	20
Case A1_m_2000	0	50.6	199.6	2000	6.51	399.2	>18	>18	0.001262	20
Case A2_m_200	0	50.6	199.6	200	0.95	39.9	37	53	0.000239	20
Case A2_m_400	0	50.6	199.6	400	1.30	79.8	60	83	0.000279	20
Case A2_m_600	0	50.6	199.6	600	1.95	119.76	85	113	0.000297	20
Case A2_m_800	0	50.6	199.6	800	2.60	159.68	112	146	0.000380	20
Case A2_m_1000	0	50.6	199.6	1000	3.26	199.6	141	180	0.000445	20
Case A2_m_1200	0	50.6	199.6	1200	3.91	239.52	173	216	0.000376	20
Case A2_m_1400	0	50.6	199.6	1400	4.56	279.44	207	254	0.000377	20
Case A2_m_1600	0	50.6	199.6	1600	5.21	319.36	243	295	0.000382	20
Case A2_m_1800	0	50.6	199.6	1800	5.86	359.28	280	337	0.000428	20
Case A2_m_2000	0	50.6	199.6	2000	6.51	399.2	320	384	0.000468	20
Case A3_m_200	0	50.6	199.6	200	0.95	39.9	69	106	0.002002	20
Case A3_m_400	0	50.6	199.6	400	1.30	79.8	113	162	0.002570	20
Case A3_m_600	0	50.6	199.6	600	1.95	119.76	157	218	0.002325	20
Case A3_m_800	0	50.6	199.6	800	2.60	159.68	203	275	0.002215	20
Case A3_m_1000	0	50.6	199.6	1000	3.26	199.6	252	336	0.001923	20
Case A3_m_1200	0	50.6	199.6	1200	3.91	239.52	304	>90	0.002065	20
Case A3_m_1400	0	50.6	199.6	1400	4.56	279.44	363	>90	0.001884	20
Case A3_m_1600	0	50.6	199.6	1600	5.21	319.36	462	>90	0.001565	20
Case A3_m_1800	0	50.6	199.6	1800	5.86	359.28	621	>90	0.001540	20
Case A3_m_2000	0	50.6	199.6	2000	6.51	399.2	866	>90	0.001675	20
Case A1_λ_100	0	50.6	100	307	1	30.7	13	25	0.000784	20
Case A1_λ_150	0	50.6	150	307	1	46.1	14	28	0.000714	20

Cases	d [mm]	T_m [°C]	λ [kJ/kg]	m [g]	L_{PCM} [mm]	$E_{\lambda,total}$ [kJ]	t_{44} [s]	t_{55} [s]	Imbalances [%]	ΔT_{mushy} [°C]
Case A1_λ_200	0	50.6	200	307	1	61.4	15	34	0.000643	20
Case A1_λ_250	0	50.6	250	307	1	76.8	16	42	0.001079	20
Case A1_λ_300	0	50.6	300	307	1	92.1	18	>60	0.001215	20
Case A2_λ_100	0	50.6	100	307	1	30.7	42	62	0.001546	20
Case A2_λ_150	0	50.6	150	307	1	46.1	46	65	0.001471	20
Case A2_λ_200	0	50.6	200	307	1	61.4	49	69	0.001756	20
Case A2_λ_250	0	50.6	250	307	1	76.8	53	72	0.001737	20
Case A2_λ_300	0	50.6	300	307	1	92.1	56	76	0.002492	20
Case A3_λ_100	0	50.6	100	307	1	30.7	76	119	0.001738	20
Case A3_λ_150	0	50.6	150	307	1	46.1	84	128	0.002197	20
Case A3_λ_200	0	50.6	200	307	1	61.4	93	136	0.00247	20
Case A3_λ_250	0	50.6	250	307	1	76.8	101	145	0.002538	20
Case A3_λ_300	0	50.6	300	307	1	92.1	110	154	0.002977	20

Annex D: Formulas and Calculations

DSC function Used

A DSC thermogram of lauric acid is reported in (a. a. F. Al-Hamadani & Shukla, 2012). An approximation to the curve was done using the following formula (Phelps & Sidhu, 2015):

$$C_{app} = \frac{dH}{dT} = \frac{d}{dT}\left[0.5 \times \lambda \times \text{erf}\left(\frac{T - T_m}{T_0}\right) + C_{PCM}(T - T_m)\right] = \lambda \times \frac{exp\left(-\frac{T - T_m}{T_0}\right)^2}{T_0\sqrt{\pi}} + C_{PCM} \quad \text{(eq.7)}$$

where C_{app} is an apparent heat capacity, λ the latent heat of the PCM, T the temperature T_m the melting temperature and T_0 the width of the mushy region and C_{PCM} is the specific heat of the PCM(Phelps & Sidhu, 2015). All parameter values were taken from (a. a. F. Al-Hamadani & Shukla, 2012), except T_0 as it was unavailable. T_0 was left as degree of freedom in a minimizing square adjustment, using the Microsoft 2013 EXCEL Solver.

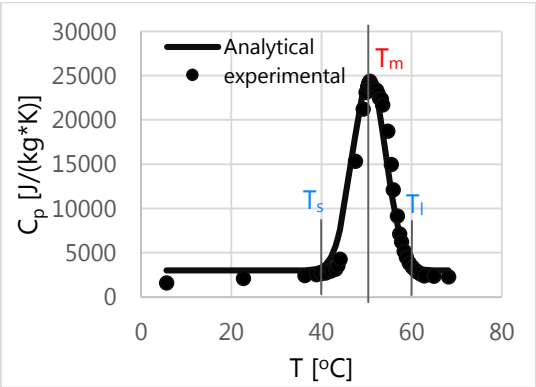

Annex Figure 3: DSC of lauric acid curve approximation using analytical expression mentioned above.

This curve adjustment was done to the experimental data obtained by a. a. F. Al-Hamadani & Shukla (2012). When the PCM mass (*m*) and position (*d*) were varied, the curve assumed was the same as it is since these variables had no influence on its shape

(equation 7). However, when the latent heat (λ) was varied, it did influence the sahpe of the curve. More specifically, the area below the peak increased. In the parametric study, for each latent heat, the Capp curve was modified accordingly, and then the simulation was run.

When the melting temperature (T_m) was varied, this also had an influence in the shape of the curve (equation 7). More specifically, for each T_m considered, the peak was shifted so that its center corresponded to the specified T_m, and then the simulation was runned.

Latent energy calculation

The latent energy used along the process is calculated according to the following formula:

$$H = 0.5 \times \lambda \times \mathrm{erf}\left(\frac{T - T_m}{T_0}\right) + C_{PCM}(T - T_m)$$

$$H_L = 0.5 \times \lambda \times \mathrm{erf}\left(\frac{T - T_m}{T_0}\right)$$

$$E_\lambda = \rho_{PCM} A \int_{x=x_1}^{x=x_2} \frac{1}{2}\lambda \mathrm{erf}\left(\frac{T - T_m}{T_0}\right) dx + \frac{1}{2}\rho_{PCM} L_{PCM} \lambda A \qquad \text{(eq.8)}$$

Where H_L represents the latent heat part of the total enthalpy, H. As seen by equation 7, the latent heat is calculated by the first term of the formula that is being derived. If this function is integrated in the PCM domain bounded by x_1 and x_2, it gives the sum of all the changes in latent heat in the individual x positions which then originates the total latent enthalpy change throughout the PCM with respect to the temperature gradient it contains. The second term is a vertical shift so that the error function varies between 0 and 1, instead of -1/2 and 1/2, so that when the latent heat is zero E_λ is also zero.

The total latent energy is calculated by:

$$E_{\lambda,total} = \rho_{PCM} L_{PCM} \lambda A \quad \text{(eq.9)}$$

where ρ_{PCM} is the density of the PCM in kg/m^3, λ the latent heat in kJ/kg, A the cross-sectional area of the PCM in m^2 , T the temperature in K, T_m the melting temperature in K, T_0 the mushy region, and L_{PCM} the length of the PCM layer in m.

Total energy calculation

$$E = A \int_{x=x_1}^{x=x_2} U \rho_{PCM} \, dx \quad \text{(eq.10)}$$

where U is the specific internal energy in kJ/kg. The internal energy equals the total enthalpy change in this case since there is no volume nor pressure changes in the domain.

Relative time calculation

It is of use to represent the time it takes for the epidermis/derrmis layer to reach 44 ºC and 55 ºC (t_{44} and t_{55}, respectively) in relative terms. The relative time it takes for the epidermis/dermis layer to reach 44 ºC is defined relative to the shortest t_{44} obtained, with respect to a variable analysis. The same goes for the relative time it takes for the epdermis/dermis layer to reach 55 ºC as shown in equation (11).

$$\tau_{44(55)} = \frac{t_{44(55)} - t_{44(55),min}}{t_{44(55),min}} \times 100 \quad \text{(eq.11)}$$

where $t_{44(55)}$ is the time it takes for the epidermis/dermis layer to reach 44 ºC or 55 ºC, $t_{44(55),min}$ is the minimum $t_{44(55)}$ obtained with respect to a variable analysis, and $\tau_{44(55)}$ represents the relative time for the epidermis/dermis layer to reach 44 ºC and 55 ºC.

Annex E: Verification of Computational Code:

Verification is the process where a numerical code's solution is compared to other solutions in the literature assuming the same physical model. Hence, if the code is written correctly, a grid-independent solution should yield almost if not the same exact solution.

The verification case that follows uses G N Mercer & Sidhu (2008) as a reference. The model the authors used was the apparent heat capcity model which is the same one used in this thesis .The geometry used is the same as the one implemented in this thesis (Figure 1). An exposure of 83.2 kW for 3 s is imposed on the left extreme boundary. The right extreme boundary was assumed to be at 37 ºC and the garment layers at 34 ºC, and a temperature gradient in the skin layers between these two temperatures was also assumed, just like in the current thesis. The PCM used is an inorganic salt that has a DSC thermogram specified in the paper. All garment layer properties (including skin properties) are the same as the ones defined in this thesis (Table 3). Blood properties were taken from Nybo et al. (2002), as these were not specified. Temperature profiles along various boundaries in the garment skin system were obtained. Annex Figure 4 shows the temperature histories obtained at the given boundaries, and the ones obtained G N Mercer & Sidhu (2008).

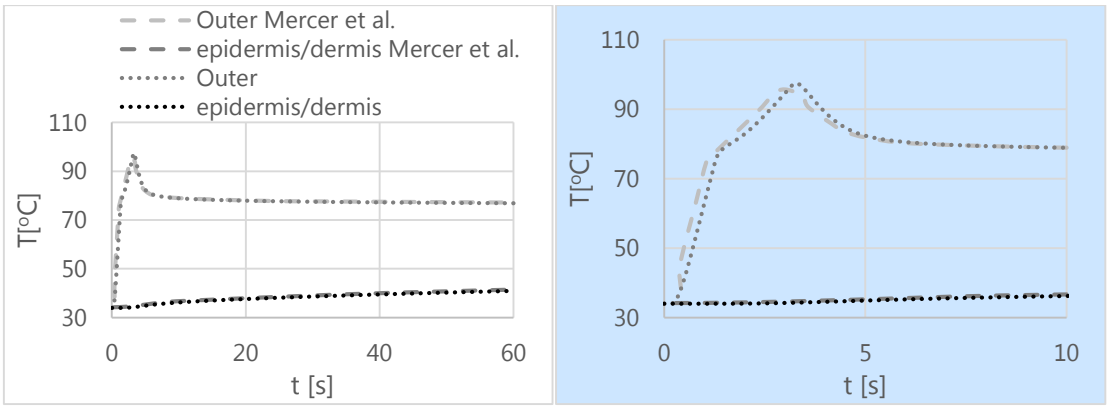

Annex Figure 4: Comparison between results obtained and the ones reported by Mercer et al.

Different time and space meshes were used to obtain grid-independent solutions. To note that energy imbalance convergence was used as a secondary criteria to claim convergence. For the outer position the solution obtained is in fair agreement with the results obtained by Mercer et al. Discrepancies between the two solutions can be related to the way the initial conditions were defined. For the epidermis/dermis layer very good agreement is registered.